

Oxidative stress-induced EGR1 upregulation promotes NR4A3-mediated nucleus pulposus cells apoptosis in intervertebral disc degeneration

Si-Kuan Zheng¹, Xiao-Kun Zhao¹, Hui Wu^{1,2,3}, Ding-Wen He^{1,2,3}, Long Xiong^{1,2,3}, Xi-Gao Cheng^{1,2,3}

¹Department of Orthopedics, The Second Affiliated Hospital, Jiangxi Medical College, Nanchang University, Nanchang, Jiangxi 330006, China

²Institute of Orthopedics of Jiangxi Province, Nanchang, Jiangxi 330006, China

³Institute of Minimally Invasive Orthopedics, Nanchang University, Nanchang, Jiangxi 330006, China

Correspondence to: Xi-Gao Cheng, Long Xiong; email: ndefy12160@ncu.edu.cn; ncxionglong2@126.com, <https://orcid.org/0000-0001-8963-674X>

Keywords: intervertebral disc degeneration, EGR1, NR4A3, nucleus pulposus, apoptosis

Received: January 10, 2024

Accepted: April 16, 2024

Published: June 28, 2024

Copyright: © 2024 Zheng et al. This is an open access article distributed under the terms of the [Creative Commons Attribution License](https://creativecommons.org/licenses/by/4.0/) (CC BY 4.0), which permits unrestricted use, distribution, and reproduction in any medium, provided the original author and source are credited.

ABSTRACT

This study aimed to reveal the specific role of early growth response protein 1 (EGR1) and nuclear receptor 4A3 (NR4A3) in nucleus pulposus cells (NPCs) and the related molecular mechanism and to identify a new strategy for treating intervertebral disc degeneration (IVDD). Bioinformatics analysis was used to explore and predict IVDD-related differentially expressed genes, and chromatin immunoprecipitation sequencing (ChIP-seq) revealed NR4A3 as the EGR1 target gene. An *in vitro* NPC model induced by tributyl hydrogen peroxide (TBHP) and a rat model induced by fibrous ring acupuncture were established. Western blotting, quantitative real-time polymerase chain reaction (qRT-PCR), immunohistochemical staining, immunofluorescence staining, and flow cytometry were used to detect the effects of EGR1 and NR4A3 knockdown and overexpression on NPC apoptosis and the expression of extracellular matrix (ECM) anabolism-related proteins. Interactions between EGR1 and NR4A3 were analyzed via ChIP-qPCR and dual luciferase assays. EGR1 and NR4A3 expression levels were significantly higher in severely degenerated discs (SDD) than in mildly degenerated discs (MDD), indicating that these genes are important risk factors in IVDD progression. ChIP-seq and RNA-seq revealed NR4A3 as a direct downstream target of EGR1, and this finding was verified by ChIP-qPCR and dual luciferase reporter experiments. Remarkably, the rescue experiments showed that EGR1 promotes TBHP-induced NPC apoptosis and impairs ECM anabolism, dependent on elevated NR4A3 expression. In summary, the EGR1-NR4A3 axis mediates the progression of NPC apoptosis and ECM impairment and is a potential therapeutic target in IVDD.

INTRODUCTION

Intervertebral disc degeneration (IVDD) is a significant cause of lower back pain (LBP) that greatly impacts patients' daily lives [1, 2]. The intervertebral disc (IVD) is a fibrous cartilage tissue located between adjacent vertebral bodies and comprises the nucleus pulposus (NP), annulus

fibrosus (AF), and cartilage endplate. Previous studies have shown that nucleus pulposus cells (NPCs) surrounded by extracellular matrix (ECM) play a crucial role in regulating IVDD [3]. Patients with IVDD accompanied by nerve or spinal cord compression symptoms often require surgical treatments, such as minimally invasive spinal surgery, intervertebral fusion surgery, or total disc replacement

surgery. However, these surgical interventions directly damage the original IVD structure and often cause complications, such as recurrent neurological symptoms and adjacent segment disc degeneration [4, 5]. The main characteristics of IVDD are the reduction or dysfunction of NPCs and the loss of ECM [6, 7]. Therefore, studying the pathological mechanism underlying the reduction in NPCs in IVDD and exploring potential therapeutic targets has important clinical and social significance.

Located within the human chromosome 5q23–31 region, early growth response protein 1 (EGR1) represents a crucial member of the early growth response protein family [8]. As a pivotal transcription factor, EGR1 encompasses an activation domain, an inhibitory region, and two Cys2 His2-type zinc finger domains. EGR1 specifically recognizes and binds target genes and regulates their transcription [8]. EGR1 is widely expressed in many cell types and participates in important physiological processes, such as cell proliferation, differentiation, invasion, and apoptosis [9–11]. When cells are stimulated by factors such as oxidative stress, growth factors, or inflammatory cytokines, EGR1 is rapidly and transiently induced to either promote or inhibit the transcription of downstream genes [12]. Previous studies have shown that EGR1 is upregulated in osteoarthritis and accelerates chondrocyte hypertrophy-induced arthritis [13]. However, the function and specific mechanism of EGR1 in intervertebral disc NPCs remain unclear.

Our research identified NR4A3 as a direct downstream target of EGR1. Nuclear receptor subfamily 4 group A member 3 (NR4A3) is an important regulator of cellular function [14, 15]. Although NR4A3 is expressed in various cell types, there is insufficient research on the function of this molecule. Recent studies have shown that NR4A3 is upregulated in cultured Ins-1 cells and human pancreatic islets treated with IL-1 β and TNF α . NR4A3 knockdown can damage cytokine-mediated cell apoptosis, and NR4A3 overexpression can induce cell apoptosis [16]. These data indicate that NR4A3 has a pro-apoptotic effect. One study demonstrated that the NR4A family affects ECM protein synthesis by regulating NF- κ B signal transduction in bone marrow cells [17]. Another suggested that NR4A3 is highly expressed in osteoarthritis and can promote inflammation and the expression of cartilage matrix degradation genes [18]. However, the biological function of NR4A3 has not been investigated in IVDD research.

Hence, the primary objective of this study was to explore the roles and molecular mechanisms of EGR1 and NR4A3 in the progression of IVDD.

MATERIALS AND METHODS

Patient samples

Ten intervertebral disc NP tissue specimens were collected from patients who underwent surgery at the Second Affiliated Hospital of Nanchang University between September 2021 and June 2023. The patients' preoperative spinal magnetic resonance imaging (MRI) data were used to grade discs; those determined to be level I or II according to the Pfirrmann classification were categorized into the control group (MDD) and were obtained from young patients with acute disc herniation or newly developed traumatic spinal fractures; discs graded as level III, IV, or V were categorized into the degenerative group (SDD) and were taken from patients diagnosed with degenerative disc disease. Follow-up visits were conducted for each patient, and clinical data were comprehensively collected, encompassing details such as patient name, age, sex, diagnosis, MRI results, body mass index (BMI), and other pertinent information (Supplementary Table 1). A trio of observers independently scrutinized the extent of IVDD using the Pfirrmann classification system. This study protocol was approved by the Ethics Committee of the Second Affiliated Hospital of Nanchang University, and written informed consent was obtained from each patient.

NPC culture and induction

The immortalized human NP cell line was procured from ScienCell Research Laboratories, Inc. NPC medium (ScienCell Research Laboratories, Carlsbad, CA, USA) supplemented with 10% fetal bovine serum and 1% penicillin/streptomycin was used to culture the NP cells. The optimal culture conditions were 37°C within a humidified chamber with 5% atmospheric CO₂. An *in vitro* NPC oxidative stress degeneration model was induced by treating the cells with 50 μ M tert-butyl hydroperoxide (TBHP) for 24 hours [19, 20].

Quantitative real-time polymerase chain reaction (qRT-PCR)

Total RNA was isolated from NPCs using TRIzol reagent (TRANS, China) according to the manufacturer's instructions. Subsequently, 500 ng of total RNA was reverse transcribed into cDNA with an RT reagent kit (Takara Bio Co., Ltd., China). qRT-PCR analysis was performed using the TB Green Premix qPCR Kit (Takara Bio Co., Ltd., China) on the Bio-Rad CFX Connect System (Bio-Rad, CA, USA). The results were calculated using relative expression levels and the $2^{-\Delta\Delta Ct}$ method. The primers used for amplification are as follows: Homo EGR1 (Forward 5'-CTAGTGAGCA

TGACCAACCCAC-3', Reverse 5'-CGCTGAGTAAAT GGGACTGCTGT-3'), Homo NR4A3 (Forward 5'-CAACAGGAACCTTCTCAGCCCTC-3', Reverse 5'-ATGGAGGCTGTTCAGGAGGTTGTA-3'), Homo GAPDH (Forward 5'-TGAAGTCAACAGCGACA CCA-3', Reverse 5'-CACCCTGTTGCTGTAGCCAA-3'), Rattus EGR1 (Forward 5'-CCATCACCTATA CTGGCCGCTTC-3', Reverse 5'-AGGTGGGTGCA GCTGAGTAAATG-3'), Rattus GAPDH (Forward 5'-GCCGAGAATCATCCCTGCAT-3', Reverse 5'-GCCTGCTTACCACCTTCTTGA-3').

***In vitro* siRNA transfection**

NPCs were plated in six-well plates and transfected with scrambled EGR1 siRNA or NR4A3 siRNA using Lipo3000 Transfection Reagent (Beijing Ju-Mei Biotechnology Co., Ltd., China) according to the manufacturer's instructions. After 48 hours, cellular lysates were isolated to determine the expression of target genes. The siRNAs were purchased from GenePharma Co., Ltd. (China). The target sequences of EGR1 and NR4A3 are as follows: Homo si-EGR1-1 (GGACAAGAAAGCAACAAA), Homo si-EGR1-2 (GGCAUACCAAGAUCACUU), Homo si-EGR1-3 (GGACCUGAAGGCCUCAAU), Homo siNR4A3-1 (GCACUCCAUGUACUUAAGC), Homo siNR4A3-2 (GCUUGAAGUACAUGG AGGUGC), Homo siNR4A3-3 (CGAUGUCAGUACUGUCGAUUU), Rattus si-EGR1 (GGACAAGAAAGCAGACAAA).

Western blotting

NPCs were lysed in an ice-cold lysis buffer (Solarbio Co., Ltd., China) and centrifuged for 15 min at 4°C, after which the supernatant was collected as the whole-cell extract. The protein content was measured using a BCA assay kit (Bioshar Co., Ltd., China), and 10 µg of total protein from each sample was separated on a 10% sodium dodecyl sulfate–polyacrylamide gel and then transferred onto a polyvinylidene fluoride membrane (Millipore, Germany). The membrane was then blocked with a solution of 5% skim milk in phosphate-buffered saline (PBS) for 1 h at room temperature before being incubated with primary antibodies against EGR1 (1:1000, Proteintech, China), NR4A3 (1:1000, Proteintech, China), GAPDH (1:5000, Proteintech, China), Bax (1:2000, HUABIO, China), Bcl-2 (1:2000, Proteintech, China), Caspase-3 (1:2000, Proteintech, China), Collagen II (1:2000, HUABIO, China), and Aggrecan (1:2000, Affinity, China) at 4°C overnight. The membranes were then washed three times for 10 min each with a solution of 0.05% Tween-20 in PBS. The membranes were subsequently incubated with secondary antibodies for 1 h at room temperature and probed using an enhanced chemiluminescence (ECL)

detection reagent. The protein bands were visualized using an ECL detection system (Tanon Science and Technology Co., Ltd.) and analyzed using ImageJ Software.

Detection of intracellular reactive oxygen species (ROS)

NPCs were cultured in T25 flasks. The experimental group cells were pretreated with TBHP (50 µM, 24 h). The culture medium was removed after treatment, and the cells were washed once with PBS. According to the kit instructions (Bestbio Co., Ltd., China), a 37°C prewarmed DCFDA (008 probe) working solution was added, and the mixture was incubated in the dark for 20–60 minutes. After incubation, the cells were washed with serum-free medium, and PBS was added for imaging under a fluorescence microscope.

Immunofluorescence staining analysis

NPCs (5 × 10⁴ cells per well) were cultured on a confocal plate and incubated at 37°C. After 24 h, the cells were fixed with 4% paraformaldehyde (400 µl/well) for 15 min, incubated in 0.5% Triton X-100/PBS for 15 min, blocked with 10% goat serum for 30 min at room temperature, and incubated with an anti-EGR1 rabbit polyclonal antibody (1:500, Proteintech, China) overnight at 4°C. After removal of the primary antibody by washing with PBS for 30 min, the cells were incubated with Alexa 488-conjugated secondary antibodies (1:500, Abcam, USA) for 1 h in the dark at room temperature. After washing with PBS for 30 min, the sections were stained with a DAPI solution for 5 min to detect the nucleus. Images of the sections were obtained with a fluorescence microscope (Olympus, Japan).

Flow cytometry

NPCs were seeded into 6-well plates and subjected to various pretreatments, such as treatment with TBHP or transfection, depending on the experimental requirements. Following pretreatment, the cells were digested with trypsin, and approximately 5 × 10⁵ cells were collected and resuspended. NPCs were then centrifuged and washed with PBS to remove the supernatant per the kit manufacturer's directions (Elabscience, China). The cell pellet was resuspended in 100 µL of diluted Annexin V Binding Buffer. Annexin V-FITC (2.5 µL) and propidium iodide (PI, 2.5 µL, 50 µg/mL) were added to this suspension. The mixture was incubated in the dark at room temperature for 20 minutes for staining. After incubation, 400 µL of diluted Annexin V binding buffer was added, and the sample was thoroughly mixed. Dual-parameter analysis was

conducted using a flow cytometer (Beckman Coulter, Inc., DxFLEX, USA), with the FITC channel set to detect Annexin V-FITC and the ECD channel set to detect PI. Gating strategies for cells double-stained with Annexin V-FITC and PI were used to distinguish among live cells, early apoptotic cells, late apoptotic cells, and necrotic cells. Annexin V⁻/PI⁻ (double-negative) indicated live cells; Annexin V⁺/PI⁻ (positive/negative) identified early apoptotic cells; Annexin V⁺/PI⁺ (double positive) marked late apoptotic or dead cells; and PI⁺ (single positive) was used to identify necrotic cells. Following data acquisition, flow cytometry analysis software (version 10, FlowJo, LLC) was used to evaluate the proportion of apoptotic cells.

RNA-seq

Human NPCs were divided into the EGR1 over-expression and control groups. Total RNA was extracted from NPCs, and RNA integrity was evaluated using an RNA Nano 6000 Assay Kit. Then, the mRNA was purified from total RNA using poly-T and amplified using PCR technology to establish the RNA database. Finally, the PCR products were purified (AMPure XP system), and library quality was assessed on an Agilent Bioanalyzer 2100 system.

ChIP-seq

Human NPCs were divided into the EGR1 over-expression and control groups. Approximately 5×10^7 NPCs were treated with 1% formaldehyde to initiate cross-linking, followed by sonication in lysis buffer. Immunoprecipitation was conducted with monoclonal antibodies against EGR1 (Cell Signaling, Inc., USA), followed by ChIP-seq. After the raw sequencing data (raw data) were obtained, the ChIP-seq data were filtered, and the high-quality sequencing data (clean data) were compared with the human genome (hg38). DeepTools software was used to visualize the coverage range of ChIP-seq data, peak annotations, average profiles, and heatmaps of peak-bound TSS regions. Significant enrichment of peaks was detected in the NR4A3 (ENST00000033847) promoter region using the R package GVIZ (<https://bioconductor.org/packages/release/bioc/html/Gviz.html>), and EGR1 effective binding sites were identified on Jaspas.

ChIP-qPCR

Human NPCs were collected and cross-linked by adding 1% formaldehyde for 15 min at room temperature. Then, the cells were incubated with glycine at room temperature for 5 minutes to terminate cross-linking and washed twice with PBS. Immuno-

precipitation was conducted with 10 μ M anti-EGR1 antibody (Cell Signaling, Inc., Rabbit. no. 4153s, USA) and 2 μ g of IgG antibody (Cell Signaling Inc., cat. no. 2729s, USA) according to the manufacturer's instructions (Millipore, MAGNA0017, Germany), followed by qRT-PCR. The primer information is shown in Supplementary Table 2.

Luciferase assay

The wild-type and mutant plasmids containing the NR4A3 promoter were constructed by Focus Bioscience Co., Ltd., in Nanchang, China. To analyze NR4A3 promoter activity, NPCs in 24-well plates were transfected with DNA containing the NR4A3 promoter and EGR1 using Lipofectamine TM 2000 (Invitrogen, Inc., USA). After 36 h of transfection, the activity of firefly and Renilla luciferases in NPCs was detected using the Dual Luciferase Reporter Gene Assay Kit (Promega, Inc., USA).

IVDD rat model

An IVDD rat model was established in Sprague-Dawley rats through fibrous ring (AF) acupuncture. Briefly, the rats were anesthetized with 1% sodium pentobarbital (100 mg/kg). After anesthesia, the tail was disinfected with iodophor, and the intervertebral disc was punctured at the level of Co6–7 at a depth of 5 mm using a 21G puncture needle. The needle was inserted into the center of the nucleus pulposus through a fibrous ring and rotated 360° for 30 seconds. EGR1 siRNA (si-EGR1 (2' O-methyl (OMe) + 5'cholesterol (chol)) and control siRNA (si-Control (2' OMe + 5'chol-modified)) (RiboBio Co., Ltd., China) were injected into Co6–7 IVDs (5 nmol; 10 μ L) at 1, 7, and 14 days after surgery. Four weeks after surgery, a X-ray examination was performed on the rats to confirm the successful establishment of the model. All procedures were approved by the Animal Ethics Committee of Nanchang University.

X-ray analysis

Preoperatively and 4 weeks postoperatively, the rats underwent X-ray analysis to determine changes in intervertebral height. In brief, the rats were placed in a prone position with their tail straight and the light perpendicular to the tail. The intervertebral disc height index (DHI) was calculated using the method described by Chen et al. [21]. The DHI measured four weeks postoperatively was compared with that measured preoperatively and is expressed as %DHI = (DHI at 4 weeks postoperatively/preoperative DHI \times 100%). All images were measured by three independent observers who were unaware of the experimental design.

Histological analysis

The NP tissues were fixed in 4% paraformaldehyde for 24 hours, decalcified, embedded in paraffin, and sectioned. For immunohistochemical (IHC) analysis, the sections were incubated with an EGR1 antibody (1:200, Proteintech), an NR4A3 antibody (1:200, Proteintech), a collagen II antibody (1:200, HUABIO), and an aggrecan antibody (1:200, Affinity) according to the manufacturer's instructions. Complete rat disc sections were stained with hematoxylin–eosin (H&E) and saffron O-fast green (SO), and images of the sections were obtained under a microscope (Olympus, Japan). The degree of disc degeneration was assessed according to the historical grading of the disc degeneration [22]. The scores were obtained by three independent observers.

Statistical analysis

All experiments were performed in triplicate. The data are presented as the mean \pm standard deviation (SD). Graphics and statistical analyses were conducted with GraphPad Prism 9.0 software. Student's *t*-test was used to compare two groups, and one-way ANOVA with Tukey's post hoc test was used to compare three or more groups. A *p*-value < 0.05 was considered to indicate significance.

RESULTS

IVDD-associated genes discovered by microarray

To examine the biological role of differentially expressed mRNAs (DEMs) in IVDD, we first analyzed the microarray profiles (GSE15227 and GSE167199) of 13 degenerative NP tissue samples and 8 non-degenerative NP tissue samples (Figure 1A, 1B). We identified 628 upregulated DEMs in the GSE15227 dataset and 603 upregulated DEMs in the GSE167199 dataset. By intersecting the two sets of upregulated differentially expressed genes that we identified with the known set of transcription factors (TFs), we obtained two candidate genes: EGR1 and ZNF300 (Figure 1C). We sorted the upregulated transcription factors with differential expression in the two datasets according to their log FC values from high to low, selected the top 20 TFs from each dataset, and calculated their intersection. Finally, we identified EGR1 as the key TF associated with IVDD (Figure 1D). We further validated the stable upregulation of EGR1 through two datasets (Figure 1E, 1F). Moreover, we performed RNA-seq on NPCs overexpressing EGR1, revealing that EGR1 is involved in various biological processes, including the apoptotic pathway (Figure 1G, 1H). Therefore, we

speculate that EGR1 potentially influences IVDD progression.

EGR1 expression is increased in human degenerative intervertebral discs and TBHP-induced NPCs

Representative magnetic resonance images of human intervertebral disc with different degrees of degeneration were obtained (Figure 2A). To investigate the role of EGR1 in IVDD, we first measured its expression in mildly (grades I and II) and severely (grades III, IV, and V) degenerated human intervertebral discs. As expected, immunohistochemistry (IHC) showed that the expression of EGR1 was significantly greater in severely degenerated discs (SDD) than in mildly degenerated discs (MDD) (Figure 2B). Western blot analysis further confirmed that EGR1 protein levels were greater in the SDD group than in the MDD group (Figure 2C, 2D). These results indicate that EGR1 expression is positively correlated with IVDD severity.

Previous studies have shown that oxidative stress is a pathological factor in IVDD progression, and TBHP is often used to construct oxidative stress-induced cell degeneration models *in vitro* [23–25]. Our study confirmed that compared with those in the control group, the intracellular ROS levels in the NPCs treated with TBHP were significantly greater, indicating that TBHP can induce oxidative stress in NPCs (Supplementary Figure 1). Therefore, we induced oxidative stress in NPCs using TBHP to construct an *in vitro* NPC degeneration model for subsequent experiments. In addition, we conducted Western blot experiments and showed that TBHP induced increased expression of EGR1 and the apoptosis-related protein Bax in NPCs and decreased expression of the antiapoptotic protein Bcl-2 and the ECM synthesis-related proteins aggrecan and collagen II, confirming that oxidative stress can lead to NPC apoptosis and the upregulation of EGR1 protein expression (Figure 2E–2J). Subsequently, qRT-PCR and immunofluorescence staining further verified that TBHP induced the upregulation of EGR1 mRNA and protein expression (Figure 2K, 2L). The above results indicate that TBHP induces an increase in ROS and apoptosis in NPCs and promotes the upregulation of EGR1 expression.

EGR1 regulates apoptosis and ECM anabolism in NPCs

We used loss-of-function and gain-of-function strategies to explore the role of EGR1 in NPCs. NPCs transfected with 3 sets of EGR1 siRNA and EGR1 siRNA1 (siEGR1-1) exhibited markedly reduced EGR1

mRNA expression (Supplementary Figure 2A). Therefore, EGR1-si1 was used in the subsequent experiments. We then examined the effect of EGR1 knockdown on TBHP-induced NPC apoptosis and

impaired ECM synthesis. The results indicated that EGR1 knockdown significantly suppressed TBHP-induced Bax expression but significantly upregulated the protein expression of Bcl-2, aggrecan, and collagen II

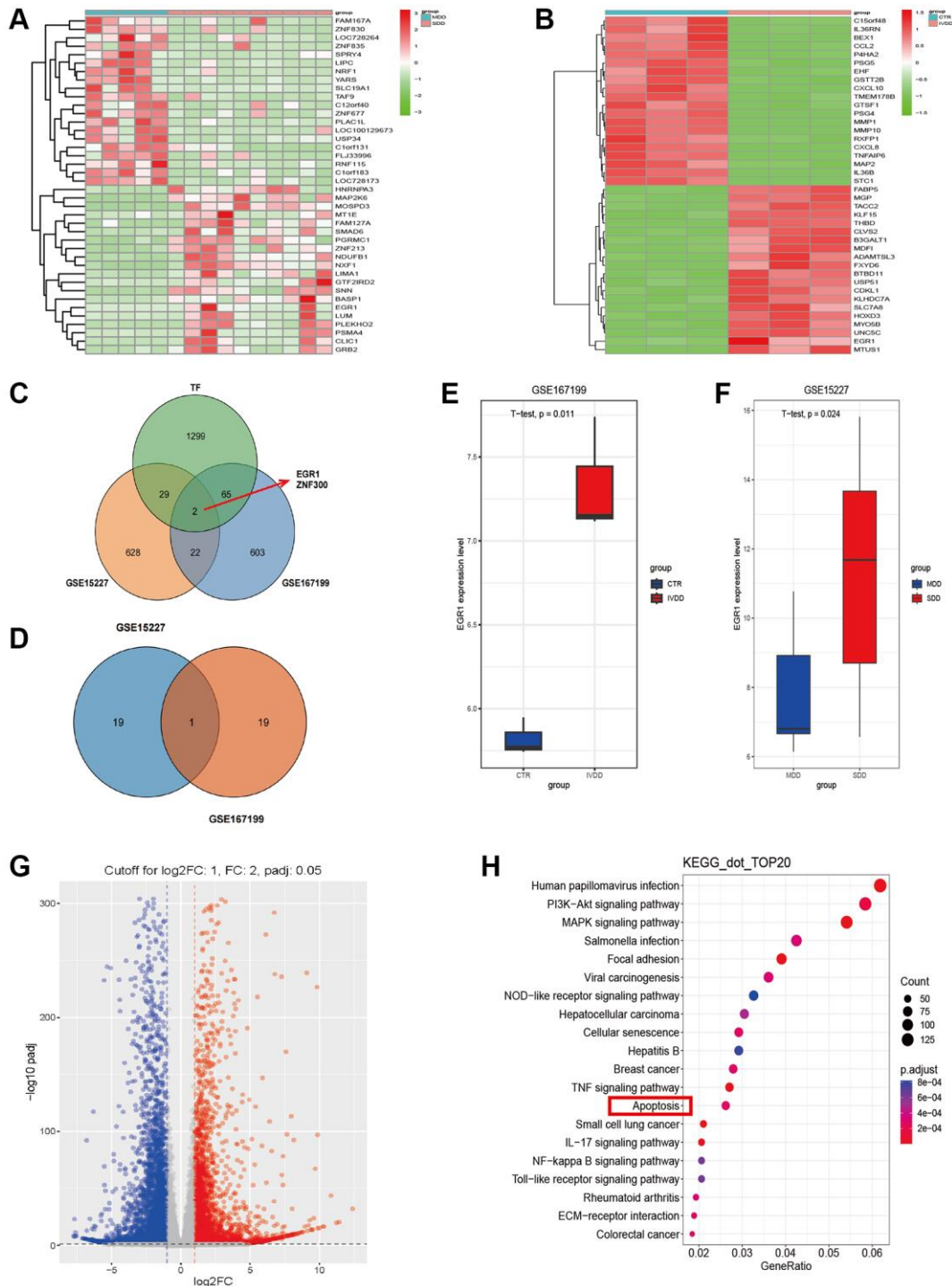


Figure 1. Abnormally expressed genes associated with IVDD identified using the GSE167199 and GSE15227 datasets. (A, B) Heatmap of all differentially expressed genes in degenerative intervertebral disc and nondegenerative intervertebral disc tissues from the GSE167199 and GSE15227 datasets. **(C)** Venn diagram showing the two selected transcription factors. **(D)** early growth response protein 1 (EGR1) was identified as a key gene. **(E, F)** EGR1 expression was analyzed by using the GSE167199 and GSE15227 datasets. **(G)** A volcano plot was created using RNA-seq data to show differentially expressed genes. **(H)** Bubble chart showing the KEGG pathway analysis of the RNA-seq data.

(Figure 3A–3E). The flow cytometry results showed that the percentage of apoptotic NPCs in the control group decreased, while that in the TBHP treatment

group significantly increased, and EGR1 siRNA antagonized TBHP-induced NPC apoptosis (Figure 3F, 3G). Therefore, knocking down EGR1 can reduce

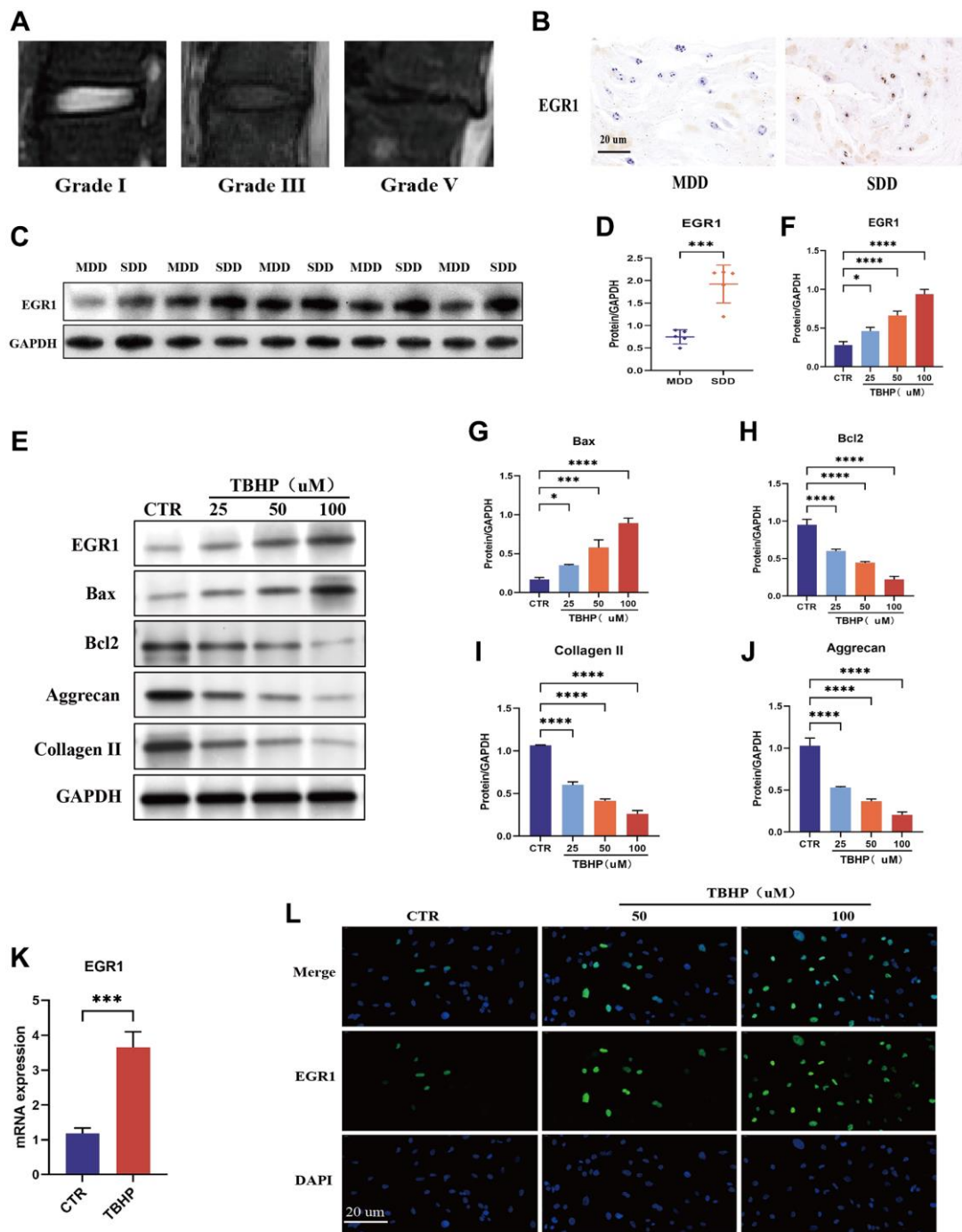


Figure 2. EGR1 expression is upregulated in human degenerative intervertebral disc tissue and in TBHP-treated NPCs. (A) Representative magnetic resonance images showing different grades of degeneration in human tissue: mild (grades I and II) and severe (grades III–V). (B) EGR1 protein expression levels were examined in severely degenerated discs (SDD) and mildly degenerated discs (MDD) by immunohistochemical (IHC) staining (magnification: $\times 400$). (C, D) The EGR1 expression level in human nucleus pulposus (NP) tissue was analyzed by western blotting. ImageJ Software was used for quantitative analysis, and the data were normalized to GAPDH. (E–J) Human nucleus pulposus cells (NPCs) were treated with different concentrations (0, 25, 50, or 100 μ M) of TBHP for 24 h, after which the proteins were extracted and the expression levels of EGR1, Bax, Bcl-2, aggrecan, and collagen II were determined by western blotting. (K) Human NPCs were treated with 50 μ M tributyl hydrogen peroxide (TBHP) for 24 h, and EGR1 mRNA expression was examined by qRT-PCR. (L) EGR1 protein expression was examined in TBHP-treated NPCs by immunofluorescence staining. * $p < 0.05$, *** $p < 0.001$, **** $p < 0.0001$.

TBHP-induced NPC apoptosis and increase ECM anabolism.

We also investigated the effects of EGR1 overexpression on TBHP-induced apoptosis and impaired

ECM synthesis. As shown in Supplementary Figure 2B, the expression of EGR1 was increased considerably in the overexpression group compared with that in the Control (CTR) group. Western blotting results indicated that EGR1 overexpression significantly increased

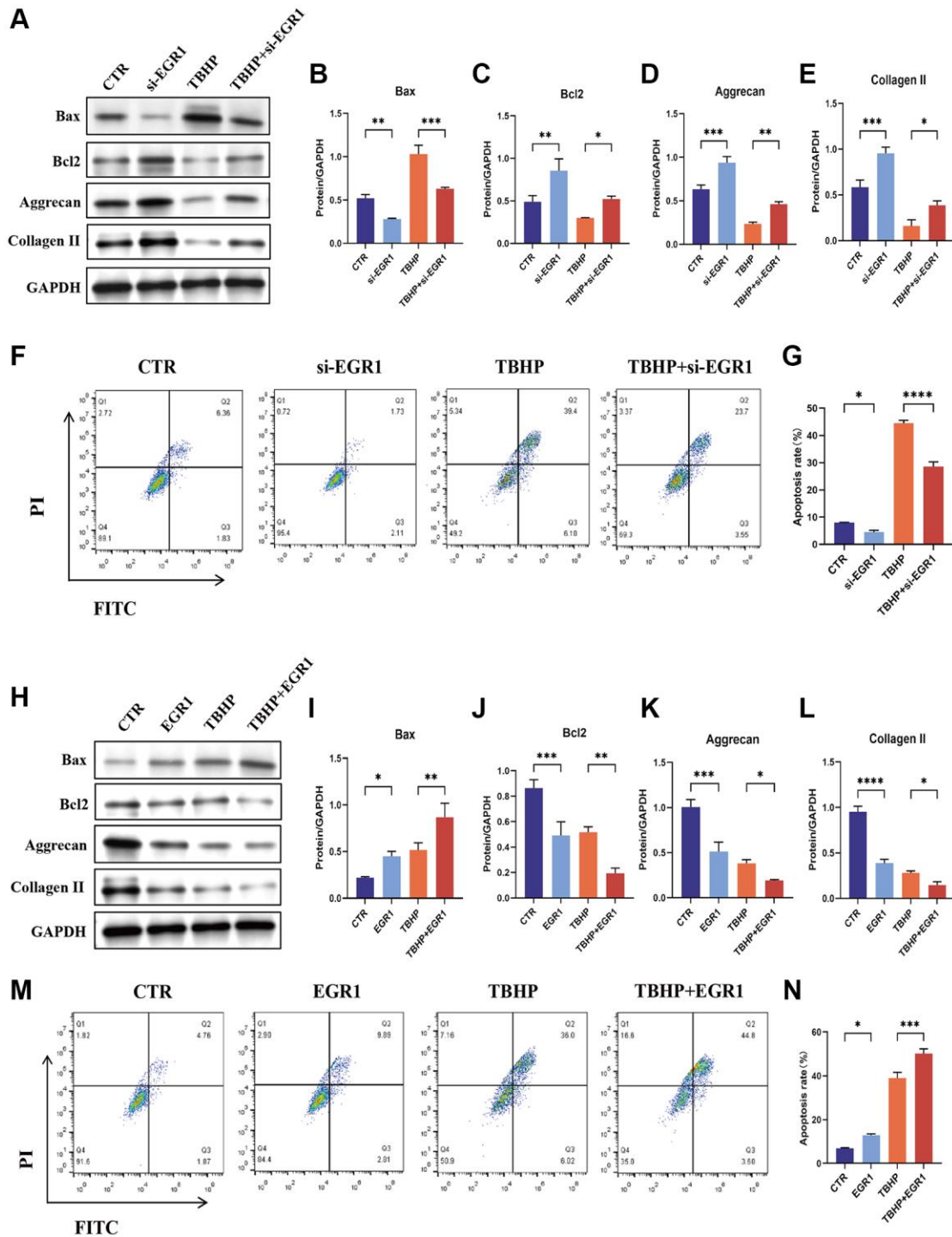


Figure 3. EGR1 regulates apoptosis and ECM synthesis in NPCs. (A) NPCs were transfected with 25 nM CTR siRNA or EGR1 siRNA-1 for 24 hours and then treated with 50 μ M TBHP for 24 hours before protein extraction. The protein expression of Bax, Bcl-2, aggrecan, and collagen II was determined by western blotting. (B–E) Quantitative analysis of Bax, Bcl-2, aggrecan, and collagen II protein levels. (F) Representative flow cytometry images showing that EGR1 siRNA protected NPCs from TBHP-induced apoptosis. (G) Quantitative analysis of the NPC apoptosis rate. (H) NPCs were transfected with 5 μ g of the EGR1 expression plasmid or the corresponding control vector. After 48 hours,

the cells were treated with 50 μ M TBHP for 24 hours. Total cellular proteins were extracted, and the expression of Bax, Bcl-2, aggrecan, and collagen II was determined by western blotting. (I–L) Quantitative analysis of Bax, Bcl-2, aggrecan, and collagen II protein levels. (M) Representative flow cytometry images showing that EGR1 overexpression increases TBHP-induced apoptosis in NPCs. (N) Quantitative analysis of the NPC apoptosis rate. The data are expressed as the mean \pm SD ($n = 3$). * $p < 0.05$, ** $p < 0.01$, *** $p < 0.001$, **** $p < 0.0001$.

TBHP-induced Bax expression but significantly decreased the protein levels of Bcl-2, aggrecan, and collagen II (Figure 3H–3L). Moreover, the flow cytometry results demonstrated that EGR1 overexpression increased TBHP-induced NPC apoptosis (Figure 3M, 3N). Taken together, these findings indicate that EGR1 overexpression can promote TBHP-induced NPC apoptosis and reduce ECM anabolic metabolism.

NR4A3 is a downstream target gene of EGR1

To explore the downstream target genes of EGR1, we screened target genes of EGR1 in human NPCs using ChIP-seq combined with RNA-seq technology. We performed a heatmap analysis of the ChIP-seq results using DeepTools software and found that the signal intensity near the transcription start site was significantly greater in the EGR1 high-expression group than that in the control group, indicating that EGR1 can bind to the promoter sequences of its target genes to exert its function in NPCs (Figure 4A). Next, we identified 32 candidate genes by intersecting 241 potential binding genes from the ChIP-seq data with 3,232 differentially upregulated genes from the RNA-seq data, excluding previously reported EGR1 target genes (Figure 4B). We constructed a protein-protein interaction network for these 32 genes and found that NR4A3, GATA2, and PLK2 strongly interact with EGR1 (Figure 4C). According to existing research reports, NR4A3 is involved in various apoptotic signaling pathways in cells [18, 26, 27]. Therefore, we speculate that NR4A3 may be a target gene through which EGR1 regulates NPC apoptosis.

To validate our hypothesis, we conducted a detailed analysis of the ChIP-seq data and identified significant peak regions near the NR4A3 promoter sequence (Figure 4D). Furthermore, by utilizing the transcription factor-binding site database JASPAR (<https://jaspar.genereg.net/>), we selected the top three binding site sequences for subsequent experimental validation according to their scores. Three potential binding sites were identified: site 1, CCTCCGCCCGCTC; site 2, CCCC GCCCACCGA; and site 3, GCTGGGGGTG GCAA (Figure 4E). To determine which NR4A3 promoter site is specifically modulated by EGR1, we performed ChIP-qPCR experiments and identified site 1 as the critical locus for EGR1-mediated transcriptional regulation of NR4A3, while sites 2 and 3 did not regulate NR4A3 expression (Figure 4F). To further

substantiate this conclusion, we constructed luciferase reporter vectors containing full-length and site 1-mutated NR4A3 promoter sequences and utilized a dual-luciferase reporter assay system to assess the impact of EGR1 overexpression on luciferase activity. The results demonstrated that EGR1 overexpression significantly enhanced the luciferase activity of the NR4A3 promoter region (Figure 4G). However, when site 1 within the NR4A3 promoter was mutated, EGR1 no longer affected promoter activity (Figure 4H). Collectively, these findings indicate that NR4A3 is a direct transcriptional target of EGR1, with EGR1 modulating NR4A3 transcriptional activity by binding to the NR4A3 promoter region.

To further explore EGR1 regulation of NR4A3, we next examined the effect of EGR1 knockdown or overexpression on NR4A3 expression. The results indicated that EGR1 knockdown significantly inhibited NR4A3 mRNA and protein expression and TBHP-induced NR4A3 mRNA and protein expression (Figure 5A–5C). In contrast, EGR1 overexpression markedly increased NR4A3 mRNA and protein expression and TBHP-induced NR4A3 mRNA and protein expression (Figure 5D–5F). Taken together, these results suggest that EGR1 positively regulates the expression of NR4A3.

NR4A3 expression is upregulated in human degenerative intervertebral discs and TBHP-treated NPCs

IHC staining revealed that the expression of NR4A3 was significantly greater in the SDD group than in the MDD group (Figure 5G). These findings were further confirmed by western blotting (Figure 5H, 5I). These results indicate that NR4A3 expression is positively correlated with IVDD severity. Moreover, qRT-PCR showed that TBHP induced NR4A3 mRNA expression in NPCs (Figure 5J). Similarly, TBHP induced NR4A3 protein expression in a concentration-dependent manner in NPCs (Figure 5K, 5L). Overall, these findings demonstrate that NR4A3 expression is upregulated in human degenerative intervertebral discs and TBHP-induced NPCs.

NR4A3 regulates apoptosis and ECM anabolism in NPCs

To investigate the function of NR4A3 in NPCs, NR4A3 was knocked down and overexpressed. NR4A3-si1 knocked down NR4A3 more effectively than the other

siRNAs (Supplementary Figure 3A). Therefore, NR4A3-si1 was used in subsequent knockdown experiments. We evaluated the impact of NR4A3 knockdown on TBHP-

induced cell apoptosis and impaired ECM synthesis. The results indicated that NR4A3 knockdown strongly downregulated TBHP-induced Bax and Caspase 3 but

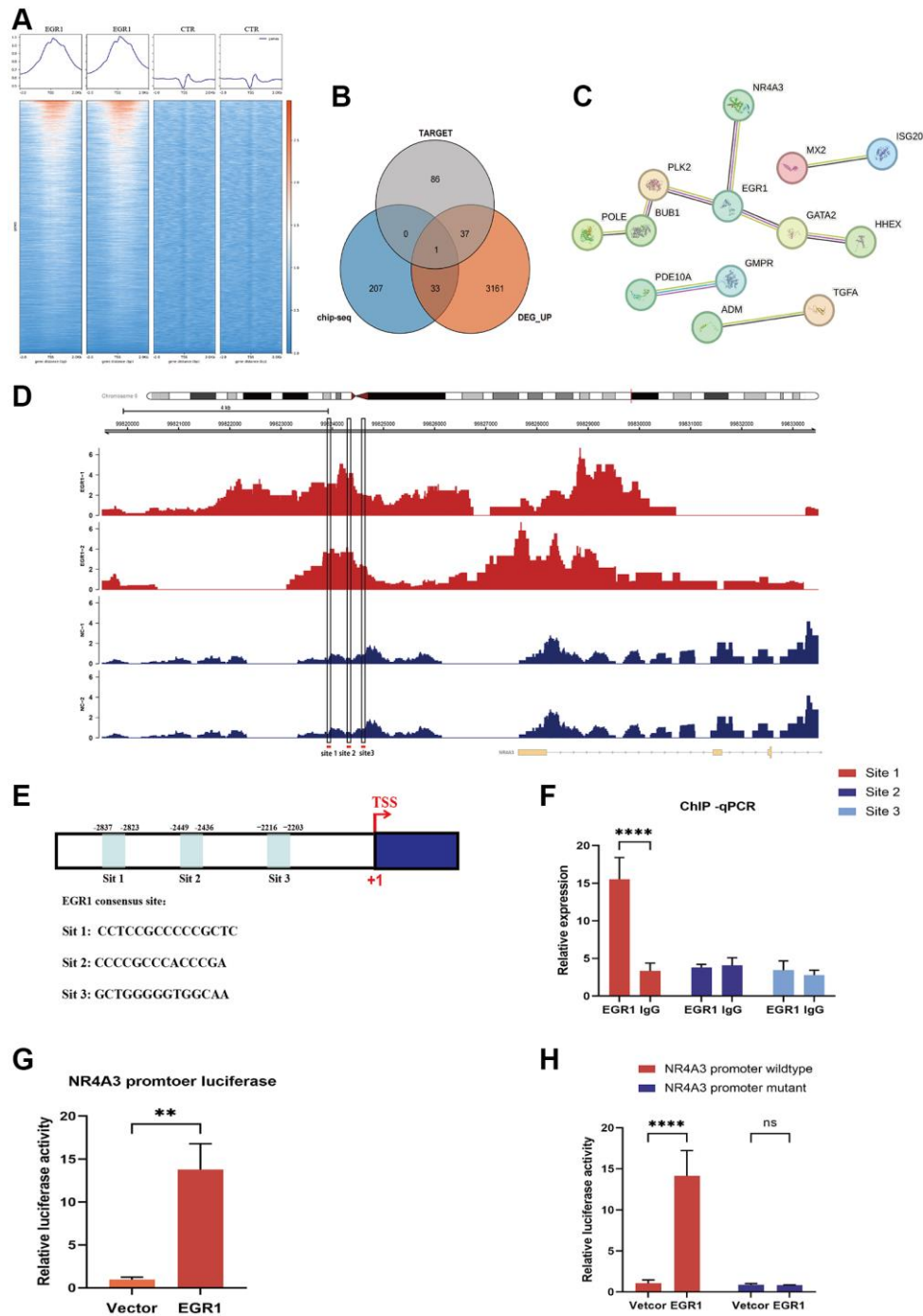


Figure 4. RNA-seq and ChIP-seq were performed to screen the downstream target genes of EGR1. (A) Heatmap analysis was performed using DeepTools software to compare the signal intensity adjacent to the transcription start site between the EGR1 overexpression and control groups. (B) Venn diagram showing screened candidate genes identified by the intersection of ChIP-seq and RNA-seq data. (C) Protein-protein interaction analysis indicating interactions between candidate genes and EGR1. (D) Potential binding sites for EGR1 on the nuclear receptor 4A3 (NR4A3) promoter were identified using the JASPAR database to analyze the ChIP-seq data. (E) Schematic diagram of three potential EGR1 binding sites (site 1, site 2, and site 3) in the NR4A3 promoter. (F) ChIP-qPCR was utilized to assess the binding of EGR1 to the NR4A3 promoter region. (G) The activation effect of EGR1 on the NR4A3 promoter was evaluated using a dual-luciferase reporter assay. (H) NPCs were transfected with plasmids containing either the full-length or site 1-mutated NR4A3 promoter to measure the luciferase activity of the NR4A3 promoter upon EGR1 overexpression. The data are expressed as the mean \pm SD ($n = 3$). ** $p < 0.01$, **** $p < 0.0001$.

markedly upregulated Bcl-2, aggrecan, and collagen II protein levels (Figure 6A, 6B). Subsequent flow cytometry analysis showed that apoptosis was

significantly increased in the TBHP-treated group, while NR4A3 knockdown partly prevented TBHP-induced apoptosis in NPCs (Figure 6C, 6D).

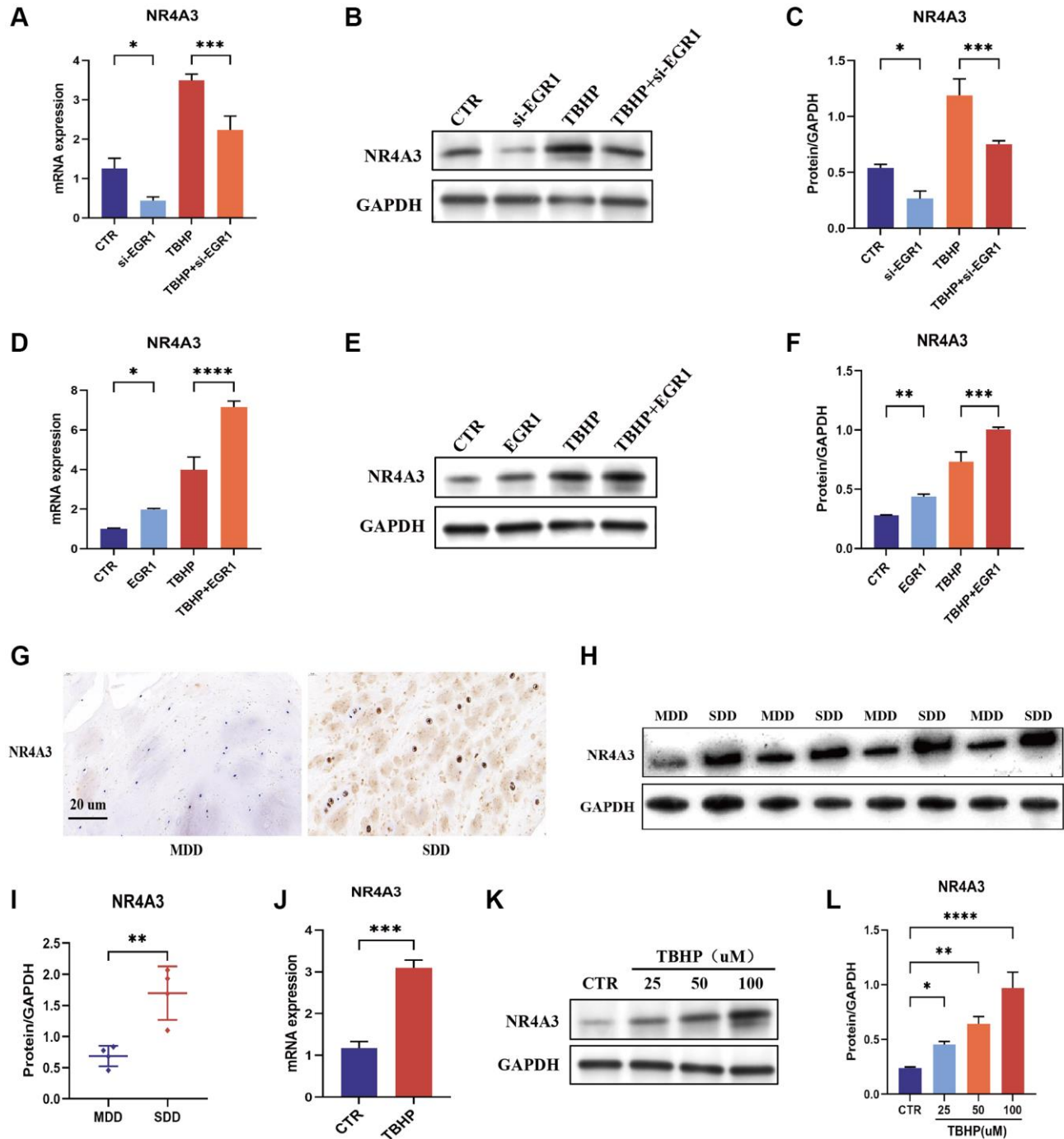


Figure 5. EGR1 positively regulates the expression of NR4A3. (A–C) NPCs were transfected with 25 nM Control siRNA or EGR1 siRNA-1 for 24 hours and then treated with 50 μ M TBHP for 24 hours before protein or mRNA extraction. The mRNA and protein expression levels of NR4A3 were determined by qRT-PCR and Western blotting. (D–F) NPCs were transfected with 5 μ g of the EGR1 expression plasmid or its control vector for 24 hours and then treated with 50 μ M TBHP for 24 hours before protein or mRNA extraction. The mRNA and protein expression of NR4A3 was determined by qRT-PCR and Western blotting. (G) The expression of NR4A3 in SDD and MDD patients was examined by IHC staining. (H) The protein expression of NR4A3 in SDD and MDD was examined by Western blotting. (I) Quantitative analysis of NR4A3 protein level in SDD and MDD. (J) The mRNA expression of NR4A3 in TBHP-treated NPCs was examined by qRT-PCR. (K) NPCs were treated with 0, 25, 50, or 100 μ M TBHP for 24 h, after which the protein was extracted, and the NR4A3 expression level was determined by Western blotting. (L) Quantitative analysis of the NR4A3 protein level. * $p < 0.05$, ** $p < 0.01$, *** $p < 0.001$, **** $p < 0.0001$.

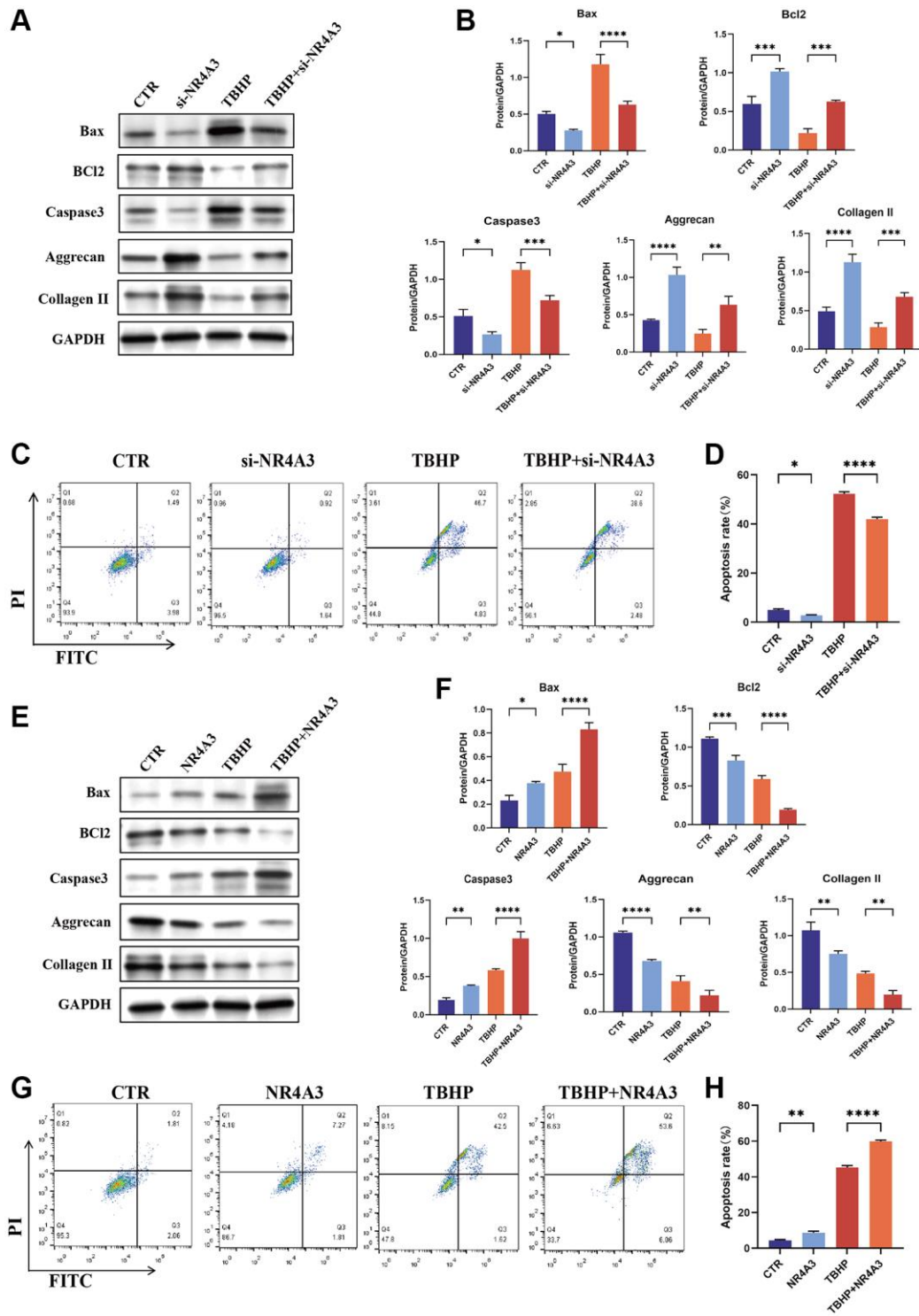


Figure 6. NR4A3 regulates NPC apoptosis and ECM synthesis. (A) NPCs were transfected with 25 nM CTR siRNA or NR4A3 siRNA-1 for 24 hours and then treated with 50 μ M TBHP for 24 hours before protein extraction. The protein expression levels of Bax, Bcl-2, caspase 3, aggrecan, and collagen II were determined by western blotting. (B) Quantitative analysis of Bax, Bcl-2, caspase 3, aggrecan, and collagen II protein levels. (C) Representative flow cytometry images showing that NR4A3 siRNA protected NPCs from TBHP-induced apoptosis. (D) Quantitative analysis of the NPC apoptosis rate. (E) NPCs were transfected with 5 μ g of the NR4A3 expression plasmid or the corresponding control vector. After 48 hours, the cells were treated with 50 μ M TBHP for 24 hours. Total cellular proteins were extracted, and the expression levels of Bax, Bcl-2, caspase-3, aggrecan, and collagen II were determined by western blotting. (F) Quantitative analysis of Bax, Bcl-2, caspase-3, aggrecan, and collagen II protein levels. (G) Representative flow cytometry images showing that overexpression of NR4A3 increased TBHP-induced apoptosis in NPCs. (H) Quantitative analysis of the NPC apoptosis rate. The data are expressed as the mean \pm SD ($n = 3$). * $p < 0.05$, ** $p < 0.01$, *** $p < 0.001$, **** $p < 0.0001$.

To further confirm these results, NPCs were transiently transfected with an NR4A3 overexpression plasmid (Supplementary Figure 3B). The results indicated that the overexpression of NR4A3 strongly increased the TBHP-induced increase in Bax and Caspase 3 but decreased the protein levels of Bcl-2, aggrecan, and collagen II (Figure 6E, 6F). Moreover, the flow cytometry results demonstrated that NR4A3 overexpression increased TBHP-induced NPC apoptosis (Figure 6G, 6H). Taken together, these findings indicate that NR4A3 can regulate apoptosis and ECM anabolism in NPCs.

EGR1 promotes NPC apoptosis in an NR4A3-dependent manner

Given the above results, we speculated that NR4A3 functions as an effector of EGR1 in IVDD progression. We then knocked down NR4A3 in NPCs over-expressing EGR1. Flow cytometry demonstrated that

knocking down NR4A3 significantly alleviated the EGR1 overexpression-induced NPC apoptosis. (Figure 7A, 7B). To confirm this conclusion, we further examined the effect of NR4A3 knockdown on EGR1 overexpression-induced apoptosis and impaired ECM anabolism by western blotting. NR4A3 knockdown strongly downregulated EGR1 overexpression-induced Bax and Caspase 3 but markedly upregulated EGR1 overexpression-inhibited Bcl-2, aggrecan, and collagen II protein levels (Figure 7C–7I). In summary, these results suggest that the promotion of apoptosis and impaired ECM synthesis metabolism in NPCs by EGR1 is contingent upon NR4A3 expression.

EGR1 siRNA alleviates the progression of IVDD by regulating NR4A3 in an IVDD rat model

To determine the role of EGR1 in the progression of IVDD *in vivo*, we injected EGR1 siRNA into an IVDD

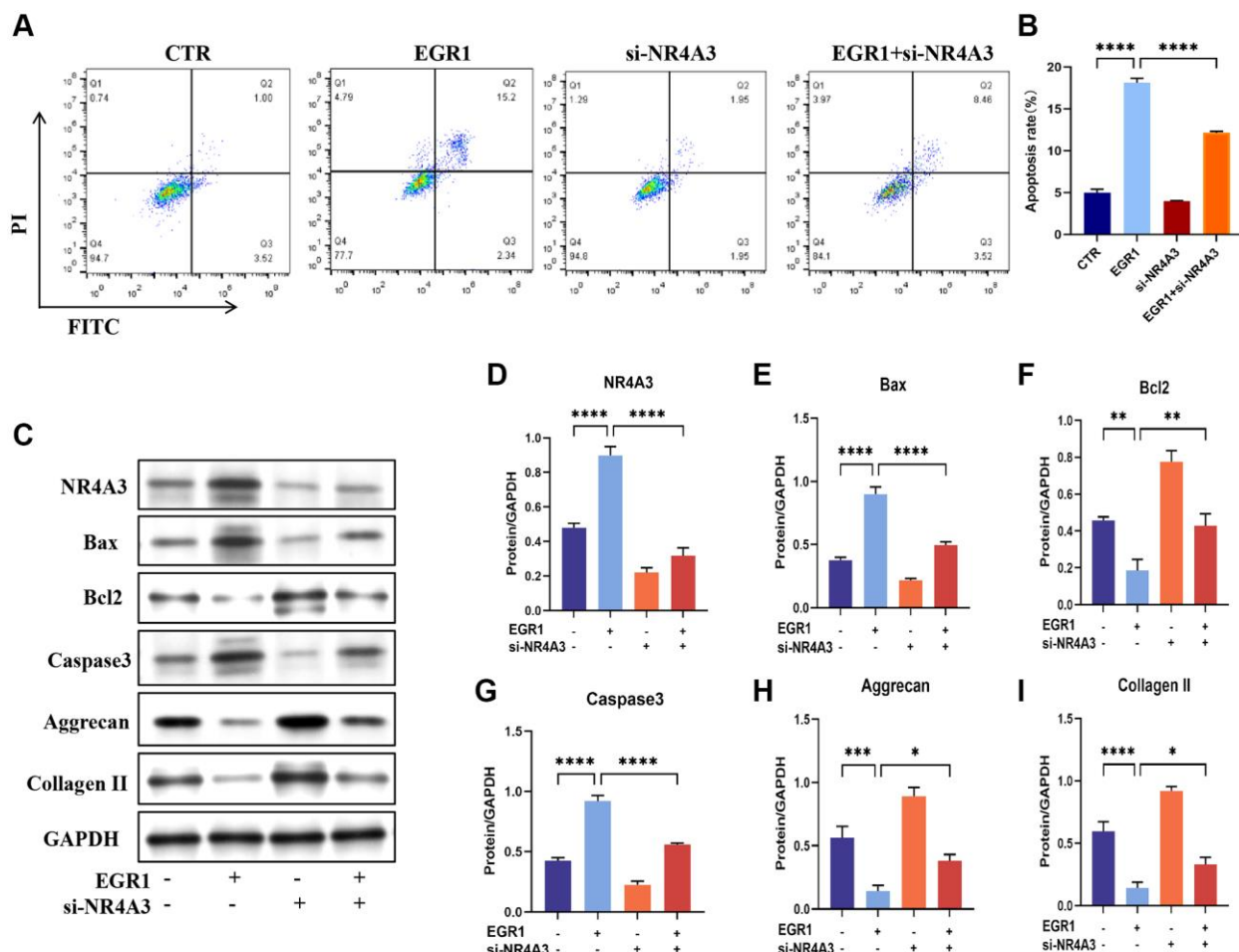


Figure 7. NR4A3 is necessary for EGR1-induced apoptosis and the impairment of ECM synthesis metabolism in human NPCs *in vitro*. (A) NPCs were transfected with EGR1 overexpression plasmids and NR4A3 siRNA, followed by flow cytometry analysis to determine the percentage of apoptotic cells in the different groups. (B) Quantitative analysis of the NPC apoptosis rate. (C) Western blot analysis was performed to determine the protein expression levels of NR4A3, Bax, Bcl-2, caspase-3, aggrecan, and collagen II in the different treatment groups. (D–I) Quantitative analysis of the NR4A3, Bax, Bcl-2, caspase-3, aggrecan, and collagen II protein levels. The data are expressed as the mean \pm SD ($n = 3$). * $p < 0.05$, ** $p < 0.01$, *** $p < 0.001$, **** $p < 0.0001$.

rat model induced by annulus fibrosus puncture (AFP). First, we examined the changes in EGR1 expression in IVDD. EGR1 protein and mRNA expression was greater in the AFP group than in the control group (Figure 8A–8C). Furthermore, an X-ray was performed 4 weeks after surgery (Figure 8D), and the results

showed that the percentage of DHI in the AFP+si-EGR1 group was significantly greater than that in the AFP and AFP+si-CTR groups (Figure 8E). This result suggested that EGR1 siRNA could slow the progression of IVDD *in vivo*. Consistent with the imaging results, H&E and S-O staining revealed a relatively indistinct boundary

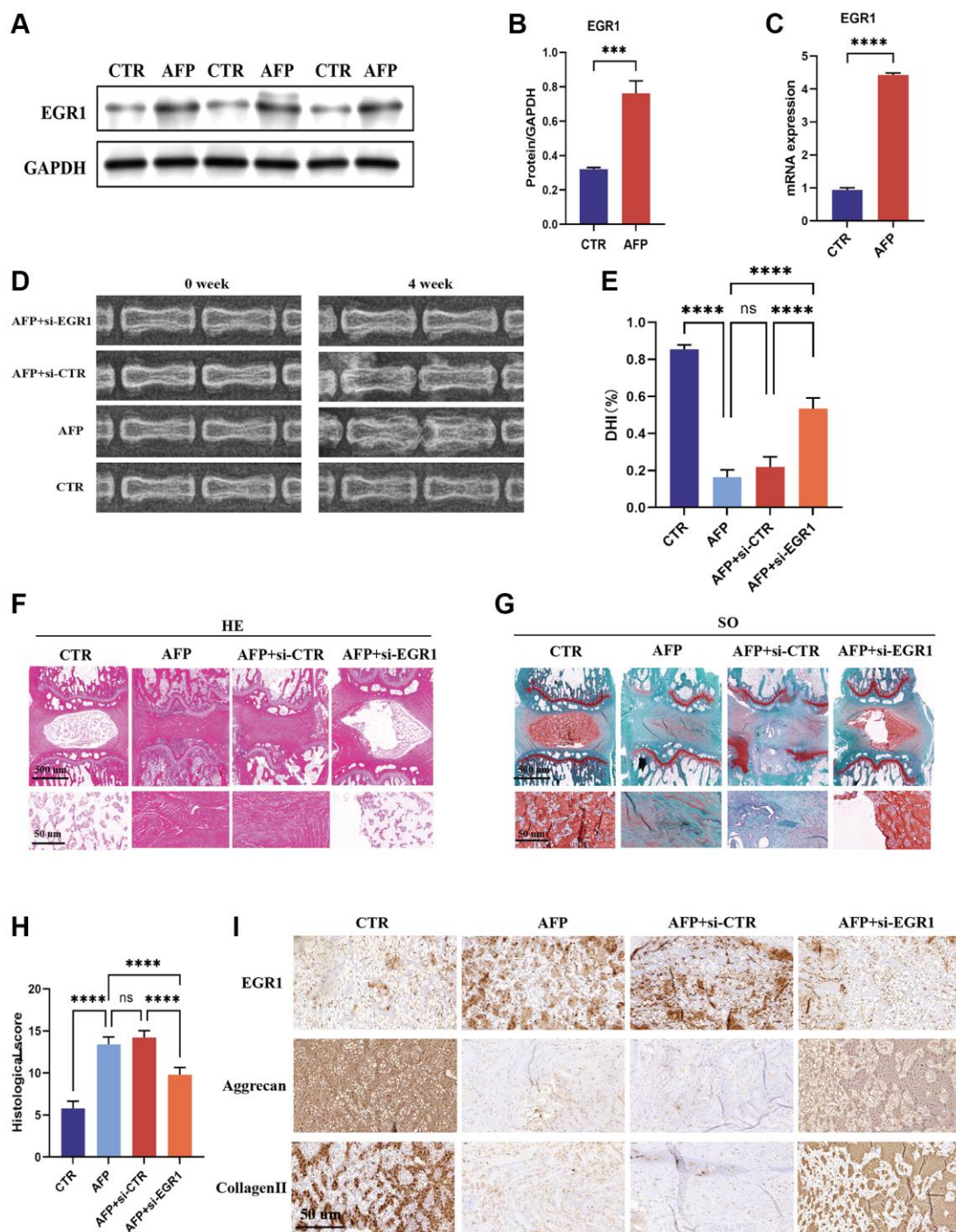


Figure 8. EGR1 siRNA alleviates the progression of IVDD in the AFP-treated rat model. (A) The protein expression of EGR1 in the IVDD rat model was determined by western blotting. (B) Quantitative analysis of EGR1 levels. (C) EGR1 mRNA expression in the IVDD rat model was examined by qRT-PCR. (D) X-ray images of the different groups before and 4 weeks after puncture. (E) Changes in intervertebral disc height were evaluated. (F, G) Representative images of HE and safranin-O staining in the four groups. (H) Histological scores were calculated. (I) Immunohistochemical staining of EGR1, aggrecan, and collagen II. *** $p < 0.001$, **** $p < 0.0001$.

between the NP and the AF and a decreased NPC number in the AFP and AFP+si-CTR groups, and this effect was alleviated in IVDD model rats treated with EGR1 siRNA (Figure 8F–8H). Similarly, IHC analysis indicated that the expression levels of aggrecan and collagen II in the AFP+si-EGR1 group were elevated relative to those in the AFP + si-CTR group (Figure 8I). Overall, these results suggest that inhibition of EGR1 has the potential to alleviate the progression of IVDD (Figure 9).

DISCUSSION

LBP is a globally recognized issue of significant academic interest and a pressing challenge in global public health. IVDD is the main cause of LBP [28]. The treatment of IVDD includes conservative and surgical strategies, but it is difficult to successfully resolve the underlying biological problem [29]. Therefore, there is an urgent need for new treatments to combat IVDD. We explored potential therapeutic targets of IVDD using bioinformatics analyses, revealing abnormal expression of EGR1 in this disease. Previous studies have shown that EGR1 is upregulated in IVDD, but the underlying mechanism is unclear [30]. Our study confirmed that NR4A3 is a direct target of EGR1 and that EGR1 regulates its transcription. Moreover, the role of EGR1 in regulating NPC apoptosis and ECM synthesis depends on NR4A3. Finally, we identified the inhibitory effect of EGR1 siRNA on the progression of IVDD *in vivo*.

The early growth response protein family is categorized by an identical protein organization encompassing four family numbers: EGR-1, EGR-2, EGR-3, and EGR-4 [31, 32]. An identical protein organization is characterized by three conserved zinc finger regions in the C-terminus that interact with target genes that harbor specific GC-rich consensus sequences [33]. The transcriptional activation domain, oriented at the N-terminus, contains binding sites for other proteins that augment the transcriptional control of EGR1. Many studies have shown that EGR1 is abnormally expressed in various diseases, such as tumors, central nervous system diseases, and cardiovascular and inflammatory diseases [34–36]. We analyzed NP samples from patients by WB and IHC and demonstrated that EGR1 expression levels positively correlate with IVDD severity. Notably, EGR1 is involved in various key biological processes as a transcription factor, such as apoptosis, proliferation, ECM metabolism, and oxidative stress [37]. For example, in prostate cells lacking the TP53 gene, EGR1 is believed to promote apoptosis by activating TNF- α [38]. During keloid formation, EGR1 responds to TGF- β and promotes ROS production by activating NADPH oxidase 4 (NOX4) [39]. Furthermore, EGR1 overexpression triggers ECM catabolism in specific embryonic fibroblasts in mice [40]. Our study also confirmed that EGR1 is significantly increased in oxidative stress-induced degenerative NPCs. Moreover, KEGG pathway analysis revealed that EGR1 upregulation is associated with the apoptosis pathway. After knocking down EGR1, the

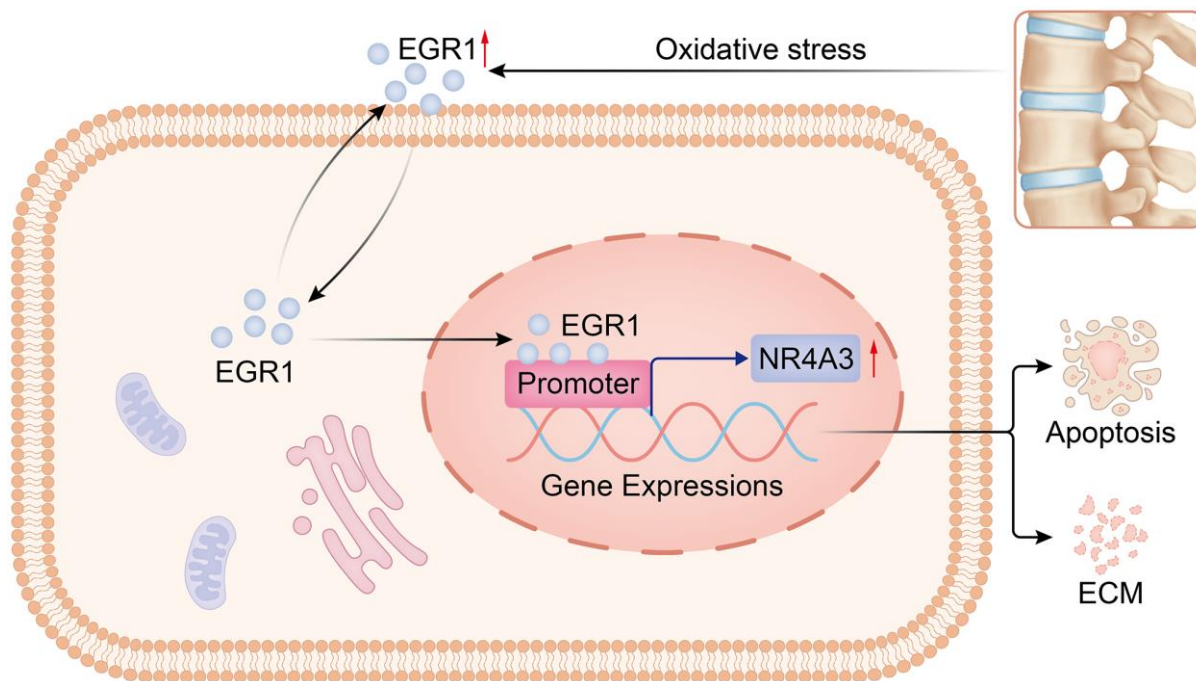


Figure 9. Diagram of the molecular mechanism by which EGR1 regulates NR4A3 in IVDD. By regulating NR4A3, EGR1 accelerates NPC apoptosis and impairs extracellular matrix anabolism, thereby promoting the progression of IVDD.

apoptosis rate in degenerative NPCs was significantly lower than that in control NPCs, and EGR1 over-expression had the opposite effect. Notably, EGR1 siRNA effectively relieved IVDD in the surgery induced IVDD rat model. Overall, these findings suggest that EGR1 is a potential therapeutic target for IVDD. Although the therapeutic effect of EGR1 siRNA on a surgery induced IVDD rat model is beneficial, the optimal dose remains to be determined, and the side effects are still unknown. Therefore, we will investigate the optimal dose and side effects in future work.

The transcription factor EGR1 has many target genes, including SOX9, SNAI2, CCND1, ABCA2, and ATF3, some of which are involved in apoptosis [41–43]. To elucidate the modulatory mechanism of EGR1 in IVDD progression, we screened the potential EGR1 target gene NR4A3 by ChIP-seq combined with RNA-seq. We found a strong interaction between NR4A3 and EGR1, which was confirmed by ChIP-qPCR and luciferase assays. NR4A3 is an immediate early gene induced by diverse stimuli, including peptide hormones, growth modulators, inflammatory cues, physiological triggers, and cellular distress [44]. The cellular levels of NR4A3 are tightly controlled under normal physiological conditions, and NR4A3 is transiently induced and activated by a diverse variety of extracellular signals, including genotoxic cellular stress, hormones, inflammatory cytokines, and metabolic, mitogenic, and apoptotic signals [45–47]. NR4A3 plays a central role in the negative selection of T lymphocytes and surface IgM-mediated and viral-induced B-cell apoptosis [48, 49]. NR4A3 has also been implicated in the regulation of proliferation, apoptosis, and cell cycle arrest in cancer cells and plays a major role in the apoptotic responses of epithelial cancer cells, including their sensitivity to antineoplastic agents [50, 51]. In the present study, we demonstrated that NR4A3 is a downstream target of EGR1 and is directly regulated by EGR1 through interactions with binding site 1 in the NR4A3 promoter. In addition, EGR1 promoted NPC apoptosis in an NR4A3-dependent manner; NR4A3 silencing reversed the effect of EGR1 on NP cell apoptosis. However, *in vivo* experiments are needed to clarify the effect of NR4A3 on IVDD. Overall, our results provide new insight into how EGR1 promotes apoptosis by regulating NR4A3.

CONCLUSION

In summary, our results showed that EGR1 knockdown could decrease the expression of NR4A3, reducing NPC apoptosis and maintaining the stability of the ECM, thereby inhibiting IVDD progression. Our research links EGR1 with NR4A3 for the first time and demonstrates the molecular mechanism regulating IVDD. In brief, our

results reveal that the EGR1-NR4A3 axis may be a potential therapeutic target in IVDD therapy.

AUTHOR CONTRIBUTIONS

The conception and design of the study were collaboratively developed by Si-Kuan Zheng, Long Xiong, and Xi-Gao Cheng. Disc specimen collection was executed by Si-Kuan Zheng and Hui Wu. Si-Kuan Zheng and Xiao-Kun Zhao undertook the cell culture and molecular biology experiments. Animal experiments were performed by Si-Kuan Zheng and Hui Wu. Data collection and analysis were carried out by Si-Kuan Zheng, Xiao-Kun Zhao, Ding-Wen He, and Hui Wu. The preparation of figures and tables for the manuscript was managed by Si-Kuan Zheng, Xiao-Kun Zhao, and Ding-Wen He. The initial manuscript draft and its subsequent revisions were edited by Si-Kuan Zheng, Long Xiong, and Xi-Gao Cheng. All authors have read and approved the final manuscript for publication, thereby ensuring the integrity and accuracy of the work.

CONFLICTS OF INTEREST

The authors declare no conflicts of interest related to this study.

ETHICAL STATEMENT AND CONSENT

This study was approved by the Biomedical Research Ethics Committee of the Second Affiliated Hospital of Nanchang University. The Ethical Examination and Approval No: Review(2023)No.(6). Written informed consent was obtained from each patient.

The experiments with animals were approved by the Animal Ethics Committee of Nanchang University, protocol number is NCULAE-20221031164.

FUNDING

This work was supported by the Thousand Talents Program of Jiangxi Province, Grant/Award Number: JXSQ2019201026. The authors extend their heartfelt gratitude to all the staff of the Department of Orthopedics at the Second Affiliated Hospital of Nanchang University for their invaluable support and assistance throughout this research.

REFERENCES

1. Richardson SM, Walker RV, Parker S, Rhodes NP, Hunt JA, Freemont AJ, Hoyland JA. Intervertebral disc cell-mediated mesenchymal stem cell differentiation. *Stem Cells*. 2006; 24:707–16. <https://doi.org/10.1634/stemcells.2005-0205> PMID:16223853

2. Walker BF. The prevalence of low back pain: a systematic review of the literature from 1966 to 1998. *J Spinal Disord.* 2000; 13:205–17.
<https://doi.org/10.1097/00002517-200006000-00003>
PMID:[10872758](https://pubmed.ncbi.nlm.nih.gov/10872758/)
3. Mern DS, Beierfuß A, Thomé C, Hegewald AA. Enhancing human nucleus pulposus cells for biological treatment approaches of degenerative intervertebral disc diseases: a systematic review. *J Tissue Eng Regen Med.* 2014; 8:925–36.
<https://doi.org/10.1002/term.1583>
PMID:[22927290](https://pubmed.ncbi.nlm.nih.gov/22927290/)
4. Chen C, Zhou T, Sun X, Han C, Zhang K, Zhao C, Li X, Tian H, Yang X, Zhou Y, Chen Z, Qin A, Zhao J. Autologous fibroblasts induce fibrosis of the nucleus pulposus to maintain the stability of degenerative intervertebral discs. *Bone Res.* 2020; 8:7.
<https://doi.org/10.1038/s41413-019-0082-7>
PMID:[32128275](https://pubmed.ncbi.nlm.nih.gov/32128275/)
5. He Y, Liu C, Huang Y. Can bone mineral density affect intra-operative blood loss of mini-invasive posterior lumbar interbody fusion? *Laparosc Endosc Robot Surg.* 2020; 3:66–9.
<https://doi.org/10.1016/j.lers.2020.06.004>
6. Rannou F, Lee TS, Zhou RH, Chin J, Lotz JC, Mayoux-Benhamou MA, Barbet JP, Chevrot A, Shyy JY. Intervertebral disc degeneration: the role of the mitochondrial pathway in annulus fibrosus cell apoptosis induced by overload. *Am J Pathol.* 2004; 164:915–24.
[https://doi.org/10.1016/S0002-9440\(10\)63179-3](https://doi.org/10.1016/S0002-9440(10)63179-3)
PMID:[14982845](https://pubmed.ncbi.nlm.nih.gov/14982845/)
7. Chen S, Liu S, Ma K, Zhao L, Lin H, Shao Z. TGF- β signaling in intervertebral disc health and disease. *Osteoarthritis Cartilage.* 2019; 27:1109–17.
<https://doi.org/10.1016/j.joca.2019.05.005>
PMID:[31132405](https://pubmed.ncbi.nlm.nih.gov/31132405/)
8. Sukhatme VP, Cao XM, Chang LC, Tsai-Morris CH, Stamenkovich D, Ferreira PC, Cohen DR, Edwards SA, Shows TB, Curran T. A zinc finger-encoding gene coregulated with c-fos during growth and differentiation, and after cellular depolarization. *Cell.* 1988; 53:37–43.
[https://doi.org/10.1016/0092-8674\(88\)90485-0](https://doi.org/10.1016/0092-8674(88)90485-0)
PMID:[3127059](https://pubmed.ncbi.nlm.nih.gov/3127059/)
9. Li TT, Liu MR, Pei DS. Friend or foe, the role of EGR-1 in cancer. *Med Oncol.* 2019; 37:7.
<https://doi.org/10.1007/s12032-019-1333-6>
PMID:[31748910](https://pubmed.ncbi.nlm.nih.gov/31748910/)
10. Rockel JS, Bernier SM, Leask A. Egr-1 inhibits the expression of extracellular matrix genes in chondrocytes by TNF α -induced MEK/ERK signalling. *Arthritis Res Ther.* 2009; 11:R8.
<https://doi.org/10.1186/ar2595>
PMID:[19144181](https://pubmed.ncbi.nlm.nih.gov/19144181/)
11. Vaish V, Piplani H, Rana C, Vaiphei K, Sanyal SN. NSAIDs may regulate EGR-1-mediated induction of reactive oxygen species and non-steroidal anti-inflammatory drug-induced gene (NAG)-1 to initiate intrinsic pathway of apoptosis for the chemoprevention of colorectal cancer. *Mol Cell Biochem.* 2013; 378:47–64.
<https://doi.org/10.1007/s11010-013-1593-y>
PMID:[23435960](https://pubmed.ncbi.nlm.nih.gov/23435960/)
12. Shin SY, Kim HW, Jang HH, Hwang YJ, Choe JS, Kim JB, Lim Y, Lee YH. γ -Oryzanol suppresses COX-2 expression by inhibiting reactive oxygen species-mediated Erk1/2 and Egr-1 signaling in LPS-stimulated RAW264.7 macrophages. *Biochem Biophys Res Commun.* 2017; 491:486–92.
<https://doi.org/10.1016/j.bbrc.2017.07.016>
PMID:[28728842](https://pubmed.ncbi.nlm.nih.gov/28728842/)
13. Sun X, Huang H, Pan X, Li S, Xie Z, Ma Y, Hu B, Wang J, Chen Z, Shi P. EGR1 promotes the cartilage degeneration and hypertrophy by activating the Krüppel-like factor 5 and β -catenin signaling. *Biochim Biophys Acta Mol Basis Dis.* 2019; 1865:2490–503.
<https://doi.org/10.1016/j.bbadis.2019.06.010>
PMID:[31201921](https://pubmed.ncbi.nlm.nih.gov/31201921/)
14. Prince LR, Prosseda SD, Higgins K, Carlring J, Prestwich EC, Ogryzko NV, Rahman A, Basran A, Falciani F, Taylor P, Renshaw SA, Whyte MKB, Sabroe I. NR4A orphan nuclear receptor family members, NR4A2 and NR4A3, regulate neutrophil number and survival. *Blood.* 2017; 130:1014–25.
<https://doi.org/10.1182/blood-2017-03-770164>
PMID:[28637666](https://pubmed.ncbi.nlm.nih.gov/28637666/)
15. McMorrow JP, Murphy EP. Inflammation: a role for NR4A orphan nuclear receptors? *Biochem Soc Trans.* 2011; 39:688–93.
<https://doi.org/10.1042/BST0390688>
PMID:[21428963](https://pubmed.ncbi.nlm.nih.gov/21428963/)
16. Close AF, Rouillard C, Buteau J. NR4A orphan nuclear receptors in glucose homeostasis: a minireview. *Diabetes Metab.* 2013; 39:478–84.
<https://doi.org/10.1016/j.diabet.2013.07.005>
PMID:[24075454](https://pubmed.ncbi.nlm.nih.gov/24075454/)
17. McEvoy C, de Gaetano M, Giffney HE, Bahar B, Cummins EP, Brennan EP, Barry M, Belton O, Godson CG, Murphy EP, Crean D. NR4A Receptors Differentially Regulate NF- κ B Signaling in Myeloid Cells. *Front Immunol.* 2017; 8:7.
<https://doi.org/10.3389/fimmu.2017.00007>
PMID:[28167941](https://pubmed.ncbi.nlm.nih.gov/28167941/)
18. Ma C, Wu L, Song L, He Y, Adel Abdo Moqbel S, Yan S, Sheng K, Wu H, Ran J, Wu L. The pro-inflammatory

- effect of NR4A3 in osteoarthritis. *J Cell Mol Med*. 2020; 24:930–40.
<https://doi.org/10.1111/jcmm.14804>
PMID:31701670
19. Chen D, Jiang X. Exosomes-derived miR-125-5p from cartilage endplate stem cells regulates autophagy and ECM metabolism in nucleus pulposus by targeting SUV38H1. *Exp Cell Res*. 2022; 414:113066.
<https://doi.org/10.1016/j.yexcr.2022.113066>
PMID:35231441
20. Wang H, Jiang Z, Pang Z, Zhou T, Gu Y. Acacetin Alleviates Inflammation and Matrix Degradation in Nucleus Pulposus Cells and Ameliorates Intervertebral Disc Degeneration in vivo. *Drug Des Devel Ther*. 2020; 14:4801–13.
<https://doi.org/10.2147/DDDT.S274812>
PMID:33204066
21. Chen Q, Yang Q, Pan C, Ding R, Wu T, Cao J, Wu H, Zhao X, Li B, Cheng X. Quiescence preconditioned nucleus pulposus stem cells alleviate intervertebral disc degeneration by enhancing cell survival via adaptive metabolism pattern in rats. *Front Bioeng Biotechnol*. 2023; 11:1073238.
<https://doi.org/10.3389/fbioe.2023.1073238>
PMID:36845177
22. Zhou X, Wang J, Fang W, Tao Y, Zhao T, Xia K, Liang C, Hua J, Li F, Chen Q. Genipin cross-linked type II collagen/chondroitin sulfate composite hydrogel-like cell delivery system induces differentiation of adipose-derived stem cells and regenerates degenerated nucleus pulposus. *Acta Biomater*. 2018; 71:496–509.
<https://doi.org/10.1016/j.actbio.2018.03.019>
PMID:29555463
23. Francisco V, Pino J, González-Gay MÁ, Lago F, Karppinen J, Tervonen O, Mobasheri A, Gualillo O. A new immunometabolic perspective of intervertebral disc degeneration. *Nat Rev Rheumatol*. 2022; 18:47–60.
<https://doi.org/10.1038/s41584-021-00713-z>
PMID:34845360
24. Wedel S, Martic I, Hrapovic N, Fabre S, Madreiter-Sokolowski CT, Haller T, Pierer G, Ploner C, Jansen-Dürr P, Cavinato M. tBHP treatment as a model for cellular senescence and pollution-induced skin aging. *Mech Ageing Dev*. 2020; 190:111318.
<https://doi.org/10.1016/j.mad.2020.111318>
PMID:32710895
25. Zhang Z, Wu J, Teng C, Wang J, Yu J, Jin C, Wang L, Wu L, Lin Z, Yu Z, Lin Z. Orientin downregulating oxidative stress-mediated endoplasmic reticulum stress and mitochondrial dysfunction through AMPK/SIRT1 pathway in rat nucleus pulposus cells in vitro and attenuated intervertebral disc degeneration in vivo. *Apoptosis*. 2022; 27:1031–48.
<https://doi.org/10.1007/s10495-022-01770-9>
PMID:36125665
26. Fedorova O, Petukhov A, Daks A, Shuvalov O, Leonova T, Vasileva E, Aksenov N, Melino G, Barlev NA. Orphan receptor NR4A3 is a novel target of p53 that contributes to apoptosis. *Oncogene*. 2019; 38:2108–22.
<https://doi.org/10.1038/s41388-018-0566-8>
PMID:30455429
27. Martínez-González J, Cañes L, Alonso J, Ballester-Servera C, Rodríguez-Sinovas A, Corrales I, Rodríguez C. NR4A3: A Key Nuclear Receptor in Vascular Biology, Cardiovascular Remodeling, and Beyond. *Int J Mol Sci*. 2021; 22:11371.
<https://doi.org/10.3390/ijms222111371>
PMID:34768801
28. Guo T, Zhang X, Hu Y, Lin M, Zhang R, Chen X, Yu D, Yao X, Wang P, Zhou H. New Hope for Treating Intervertebral Disc Degeneration: Microsphere-Based Delivery System. *Front Bioeng Biotechnol*. 2022; 10:933901.
<https://doi.org/10.3389/fbioe.2022.933901>
PMID:35928951
29. Kamali A, Ziadlou R, Lang G, Pfannkuche J, Cui S, Li Z, Richards RG, Alini M, Grad S. Small molecule-based treatment approaches for intervertebral disc degeneration: Current options and future directions. *Theranostics*. 2021; 11:27–47.
<https://doi.org/10.7150/thno.48987>
PMID:33391459
30. van den Akker GG, Surtel DA, Cremers A, Hoes MF, Caron MM, Richardson SM, Rodrigues-Pinto R, van Rhijn LW, Hoyland JA, Welting TJ, Voncken JW. EGR1 controls divergent cellular responses of distinctive nucleus pulposus cell types. *BMC Musculoskelet Disord*. 2016; 17:124.
<https://doi.org/10.1186/s12891-016-0979-x>
PMID:26975996
31. Braddock M. The transcription factor Egr-1: a potential drug in wound healing and tissue repair. *Ann Med*. 2001; 33:313–8.
<https://doi.org/10.3109/07853890109002083>
PMID:11491188
32. Thiel G, Rössler OG. Resveratrol regulates gene transcription via activation of stimulus-responsive transcription factors. *Pharmacol Res*. 2017; 117:166–76.
<https://doi.org/10.1016/j.phrs.2016.12.029>
PMID:28012964
33. Bhattacharyya S, Fang F, Tourtellotte W, Varga J. Egr-1: new conductor for the tissue repair orchestra directs harmony (regeneration) or cacophony (fibrosis). *J Pathol*. 2013; 229:286–97.

- <https://doi.org/10.1002/path.4131>
PMID:[23132749](https://pubmed.ncbi.nlm.nih.gov/23132749/)
34. Khachigian LM. Early Growth Response-1, an Integrative Sensor in Cardiovascular and Inflammatory Disease. *J Am Heart Assoc.* 2021; 10:e023539.
<https://doi.org/10.1161/JAHA.121.023539>
PMID:[34755520](https://pubmed.ncbi.nlm.nih.gov/34755520/)
35. Fisch KM, Gamini R, Alvarez-Garcia O, Akagi R, Saito M, Muramatsu Y, Sasho T, Koziol JA, Su AI, Lotz MK. Identification of transcription factors responsible for dysregulated networks in human osteoarthritis cartilage by global gene expression analysis. *Osteoarthritis Cartilage.* 2018; 26:1531–8.
<https://doi.org/10.1016/j.joca.2018.07.012>
PMID:[30081074](https://pubmed.ncbi.nlm.nih.gov/30081074/)
36. Aliperti V, Sgueglia G, Aniello F, Vitale E, Fucci L, Donizetti A. Identification, Characterization, and Regulatory Mechanisms of a Novel EGR1 Splicing Isoform. *Int J Mol Sci.* 2019; 20:1548.
<https://doi.org/10.3390/ijms20071548>
PMID:[30925677](https://pubmed.ncbi.nlm.nih.gov/30925677/)
37. Wang B, Guo H, Yu H, Chen Y, Xu H, Zhao G. The Role of the Transcription Factor EGR1 in Cancer. *Front Oncol.* 2021; 11:642547.
<https://doi.org/10.3389/fonc.2021.642547>
PMID:[33842351](https://pubmed.ncbi.nlm.nih.gov/33842351/)
38. Ahmed MM, Sells SF, Venkatasubbarao K, Fruitwala SM, Muthukkumar S, Harp C, Mohiuddin M, Rangnekar VM. Ionizing radiation-inducible apoptosis in the absence of p53 linked to transcription factor EGR-1. *J Biol Chem.* 1997; 272:33056–61.
<https://doi.org/10.1074/jbc.272.52.33056>
PMID:[9407088](https://pubmed.ncbi.nlm.nih.gov/9407088/)
39. Qin H, Zhang L, Li M, Liu Y, Sun S, Nie W, Bai B, Li G, Zhang G. EGR1/NOX4 pathway regulates oxidative stress and further facilitates fibrosis progression in keloids responses to TGF- β 1. *J Dermatol Sci.* 2022; 108:138–45.
<https://doi.org/10.1016/j.jdermsci.2022.12.009>
PMID:[36608994](https://pubmed.ncbi.nlm.nih.gov/36608994/)
40. Ai K, Li X, Zhang P, Pan J, Li H, He Z, Zhang H, Yi L, Kang Y, Wang Y, Chen J, Li Y, Xiang X, et al. Genetic or siRNA inhibition of MBD2 attenuates the UUO- and I/R-induced renal fibrosis via downregulation of EGR1. *Mol Ther Nucleic Acids.* 2022; 28:77–86.
<https://doi.org/10.1016/j.omtn.2022.02.015>
PMID:[35356685](https://pubmed.ncbi.nlm.nih.gov/35356685/)
41. Wang Y, Qin C, Zhao B, Li Z, Li T, Yang X, Zhao Y, Wang W. EGR1 induces EMT in pancreatic cancer via a P300/SNAI2 pathway. *J Transl Med.* 2023; 21:201.
<https://doi.org/10.1186/s12967-023-04043-4>
PMID:[36932397](https://pubmed.ncbi.nlm.nih.gov/36932397/)
42. Chen JW, Huang MJ, Chen XN, Wu LL, Li QG, Hong Q, Wu J, Li F, Chen LM, Dong Y, Cai GY, Bai XY, Li Z, Chen XM. Transient upregulation of EGR1 signaling enhances kidney repair by activating SOX9⁺ renal tubular cells. *Theranostics.* 2022; 12:5434–50.
<https://doi.org/10.7150/thno.73426>
PMID:[35910788](https://pubmed.ncbi.nlm.nih.gov/35910788/)
43. Chen DG, Zhu B, Lv SQ, Zhu H, Tang J, Huang C, Li Q, Zhou P, Wang DL, Li GH. Inhibition of EGR1 inhibits glioma proliferation by targeting CCND1 promoter. *J Exp Clin Cancer Res.* 2017; 36:186.
<https://doi.org/10.1186/s13046-017-0656-4>
PMID:[29246166](https://pubmed.ncbi.nlm.nih.gov/29246166/)
44. Crean D, Murphy EP. Targeting NR4A Nuclear Receptors to Control Stromal Cell Inflammation, Metabolism, Angiogenesis, and Tumorigenesis. *Front Cell Dev Biol.* 2021; 9:589770.
<https://doi.org/10.3389/fcell.2021.589770>
PMID:[33634114](https://pubmed.ncbi.nlm.nih.gov/33634114/)
45. Wansa KD, Harris JM, Yan G, Ordentlich P, Muscat GE. The AF-1 domain of the orphan nuclear receptor NOR-1 mediates trans-activation, coactivator recruitment, and activation by the purine anti-metabolite 6-mercaptopurine. *J Biol Chem.* 2003; 278:24776–90.
<https://doi.org/10.1074/jbc.M300088200>
PMID:[12709428](https://pubmed.ncbi.nlm.nih.gov/12709428/)
46. Wansa KD, Muscat GE. TRAP220 is modulated by the antineoplastic agent 6-Mercaptopurine, and mediates the activation of the NR4A subgroup of nuclear receptors. *J Mol Endocrinol.* 2005; 34:835–48.
<https://doi.org/10.1677/jme.1.01739>
PMID:[15956351](https://pubmed.ncbi.nlm.nih.gov/15956351/)
47. Smith AG, Luk N, Newton RA, Roberts DW, Sturm RA, Muscat GE. Melanocortin-1 receptor signaling markedly induces the expression of the NR4A nuclear receptor subgroup in melanocytic cells. *J Biol Chem.* 2008; 283:12564–70.
<https://doi.org/10.1074/jbc.M800480200>
PMID:[18292087](https://pubmed.ncbi.nlm.nih.gov/18292087/)
48. Mapara MY, Weinmann P, Bommert K, Daniel PT, Bargou R, Dörken B. Involvement of NAK-1, the human nur77 homologue, in surface IgM-mediated apoptosis in Burkitt lymphoma cell line BL41. *Eur J Immunol.* 1995; 25:2506–10.
<https://doi.org/10.1002/eji.1830250915>
PMID:[7589118](https://pubmed.ncbi.nlm.nih.gov/7589118/)
49. Lee JM, Lee KH, Weidner M, Osborne BA, Hayward SD. Epstein-Barr virus EBNA2 blocks Nur77-mediated apoptosis. *Proc Natl Acad Sci U S A.* 2002; 99:11878–83.
<https://doi.org/10.1073/pnas.182552499>
PMID:[12195020](https://pubmed.ncbi.nlm.nih.gov/12195020/)

50. Wu Q, Liu S, Ye XF, Huang ZW, Su WJ. Dual roles of Nur77 in selective regulation of apoptosis and cell cycle by TPA and ATRA in gastric cancer cells. *Carcinogenesis*. 2002; 23:1583–92.

<https://doi.org/10.1093/carcin/23.10.1583>

PMID:[12376465](https://pubmed.ncbi.nlm.nih.gov/12376465/)

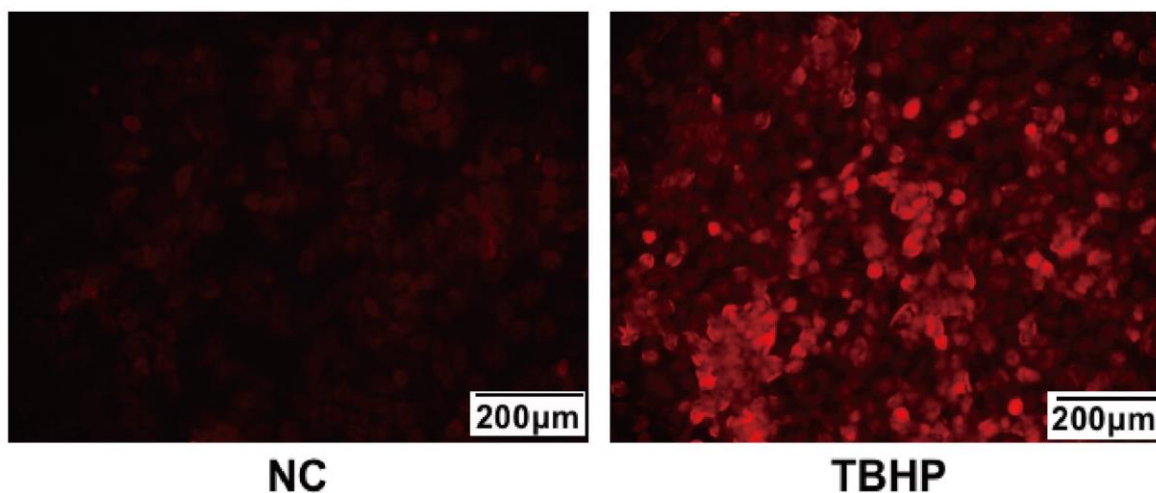
51. Uemura H, Chang C. Antisense TR3 orphan receptor can increase prostate cancer cell viability with etoposide treatment. *Endocrinology*. 1998; 139:2329–34.

<https://doi.org/10.1210/endo.139.5.5969>

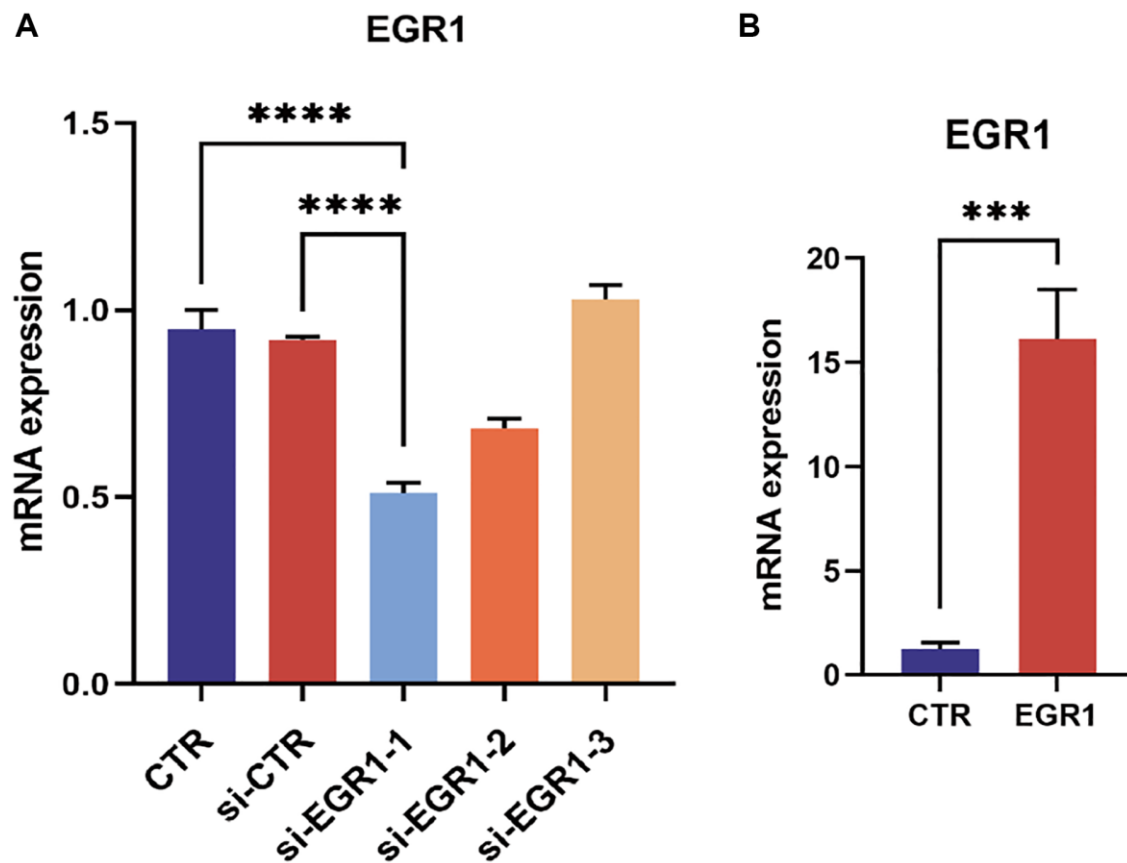
PMID:[9564841](https://pubmed.ncbi.nlm.nih.gov/9564841/)

SUPPLEMENTARY MATERIALS

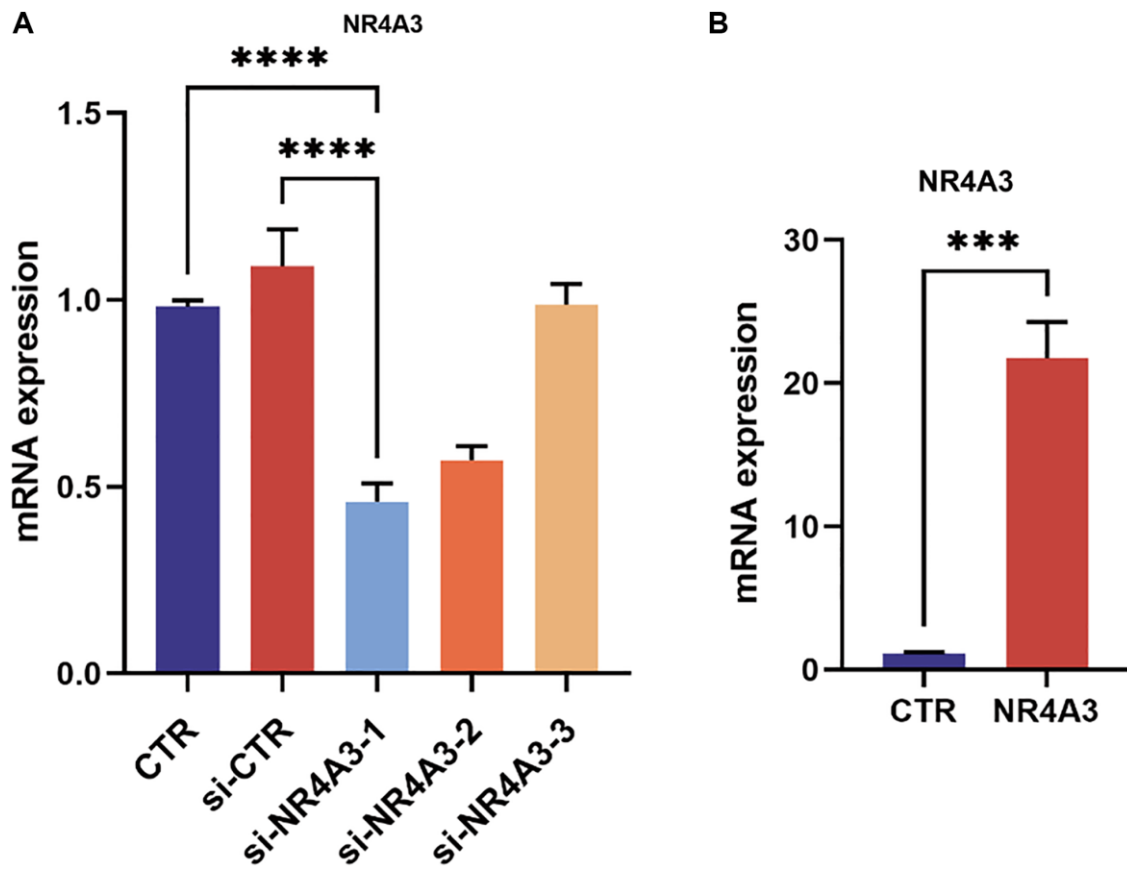
Supplementary Figures



Supplementary Figure 1. Reactive oxygen species levels in NPCs. The control group consisted of normal NPCs, while the experimental group consisted of NPCs induced with TBHP (50 μ M, 24 h). The difference in reactive oxygen species levels between the two groups was compared under a fluorescence microscope.



Supplementary Figure 2. Efficiency of EGR1 knockdown and overexpression. (A) mRNA levels in NPCs after transfection with different EGR1 siRNAs. (B) mRNA levels in NPCs after transient transfection with plasmids overexpressing EGR1. The data are expressed as the mean \pm SD ($n = 3$). *** $p < 0.001$, **** $p < 0.0001$.



Supplementary Figure 3. Efficiency of NR4A3 knockdown and overexpression. (A) mRNA levels in NPCs after transfection with different NR4A3 siRNAs. (B) mRNA levels in NPCs after transient transfection with plasmids overexpressing NR4A3. The data are expressed as the mean \pm SD ($n = 3$). *** $p < 0.001$, **** $p < 0.0001$.

Supplementary Tables

Supplementary Table 1. Information on human disc samples from 10 patients.

Samples	Diagnosis	Sex	Age	BMI	Level	Grade
1	Acute disc herniation	M	19y	23.7	L4/L5	II
2	Acute disc herniation	M	18y	24.1	L4/L5	I
3	Acute disc herniation	M	28y	25.3	L4/L5	II
4	Spinal fractures	F	33y	20.7	T12/L1	I
5	Acute disc herniation	F	16y	23.5	L5/S1	I
6	Degenerative disc disease	F	51y	27.5	L5/S1	III
7	Degenerative disc disease	F	80y	22.1	L4/L5	V
8	Degenerative disc disease	M	66y	26.4	L4/L5	V
9	Degenerative disc disease	M	67y	18.4	L4/L5	V
10	Degenerative disc disease	M	62y	26.2	L5/S1	IV

Abbreviations: M: male; F: female, y: year.

Supplementary Table 2. Primer sequence for ChIP-qPCR.

Site	Gene	Primer sequence
Site 1	NR4A3-ChIP-F1	GAATCTCAGTCTTCCCTTTCTGTC
	NR4A3-ChIP-R1	TGGGCAGACGAAAGGAACAC
Site 2	NR4A3-ChIP-F2	GAGGAAAGGCTGTGTGGGTC
	NR4A3-ChIP-R2	GCATTCCCTGAGGGCCTTTC
Site 3	NR4A3-ChIP-F3	TGGGAAGATCCGCTTCTACC
	NR4A3-ChIP-R3	GAGAAAGGGACTCGGGGCTC